Monthly Notices of the ROYAL ASTRONOMICAL SOCIETY

MNRAS **549,** 1–18 (2026)
Advance Access publication 2026 June 13

https://doi.org/10.1093/mnras/stag1137

Confirming membership in Local Group galaxies with the Dark Energy Spectroscopic Instrument Data Release 1

Federico Sestito ★ and Chiaki Kobayashi

Centre for Astrophysics Research, Department of Physics, Astronomy and Mathematics, University of Hertfordshire, Hatfield AL10 9AB, UK

Accepted 2026 June 12. Received 2026 June 9; in original form 2025 December 15

ABSTRACT

We use the Dark Energy Spectroscopic Instrument Data Release 1 (DESI DR1) to identify stellar members of the Local Group dwarf galaxies. We cross-match DESI targets with candidate members that are based on *Gaia* proper motions, positions, and photometry. The addition of DESI radial velocities enables secure membership determination in 15 systems. Our results confirm that *Gaia*-based selection algorithms are effective in minimising foreground contamination. Two stars are found to be associated with DES J0225+0304; if this is the case, then it leads to the first determination of the systemic radial velocity ($RV_{sys} = -150.0 \pm 7.0$ km s^{-1}). Draco and Sextans are the galaxies with the largest number of members. We focus on Sextans and, for the first time with DESI, trace its stellar kinematics to large radii (up to ∼10 half-light radii). We find that the metal-poor population exhibits a higher velocity dispersion and extends to larger radii, whereas the metal-rich population is kinematically colder and centrally concentrated. The metallicity gradient is steeper in the inner regions of Sextans ($\sim -12 \times 10^{-3}$ dex arcmin^{-1} or ~ -0.36 dex kpc^{-1}), while almost no gradient in the outskirts, hinting for an ex-situ halo or for an 'outside-in' star formation. Although DESI [α/Fe] ratios for Sextans stars with [Fe/H] $\gtrsim -2.0$ are in line with literature values, those for very metal-poor stars ([Fe/H] $\lesssim -2.0$) present a large scatter and strong anticorrelation with metallicity, warranting a caution for using DESI abundances in this regime. With a less strict selection, we identify 8 ultra metal-poor ([Fe/H] < -4) candidates that require higher signal-to-noise ratio spectroscopic observations to determine their metallicities.

Key words: surveys – galaxies: abundances – galaxies: dwarf – galaxies: general – Local Group – galaxies: stellar content.

1 INTRODUCTION

Nearby dwarf galaxies offer a unique laboratory for understanding galaxy formation and evolution (e.g. E. Tolstoy, V. Hill & M. Tosi 2009; J. S. Bullock & M. Boylan-Kolchin 2017; J. D. Simon 2019), as only in the Local Group it is possible to derive detailed chemodynamical information of *individual* member stars. Such low-mass systems could be the building blocks of the Milky Way, or might be analogues of the first galaxies in the early Universe. Cosmological simulations with the standard Lambda cold dark matter (Λ−CDM) cosmology seemed to overproduce dwarf satellite galaxies in the Milky Way halo, especially at the low-mass end (the so-called missing satellites problem; e.g. A. Klypin et al. 1999; B. Moore et al. 1999). This tension has now be solved with high-resolution hydrodynamical simulations including baryonic physics (e.g. L. V. Sales, A. Wetzel & A. Fattahi 2022; I. M. E. Santos-Santos, C. S. Frenk & J. F. Navarro 2026), as well as with the discovery of new systems thanks to the advent of various surveys, e.g. the Sloan Digital Sky Survey (SDSS; D. G. York et al. 2000; B. Willman et al. 2005), the Dark Energy Survey (DES; The Dark Energy Survey Collaboration 2005), Pan-STARSS1 (K. C. Chambers et al. 2016), UNIONS (S. E. T. Smith et al. 2023; S. Gwyn et al. 2025), the Hyper Suprime–Cam Subaru Strategic Program (HSC–SSP; H. Aihara et al. 2018), *Gaia* (Gaia Collaboration 2016; G. Torrealba et al. 2019), and DELVE (A. Drlica-Wagner et al. 2021). However, there is another problem related to the density and kinematics of stars in the inner regions of dwarf galaxies, i.e. the core-cusp problem (e.g. R. A. Flores & J. R. Primack 1994; J. F. Navarro, V. R. Eke & C. S. Frenk 1996; A. Genina et al. 2018); the diversity of densities among various dwarf galaxies still remains an open question to be addressed (e.g. L. V. Sales et al. 2022).

Spectroscopic observations of dwarf galaxies in the Local Group are expensive as these systems are intrinsically faint with low surface brightness, in addition to large distance from us. Hence, the number of observed stars with detailed spectroscopic information is limited and mostly confined to the inner parts of the systems. Thanks to the photometry, the exquisite proper motion, and the positions of stars from the recent data releases of *Gaia* (Gaia Collaboration 2016, 2018, 2023), it is now possible to select candidate members stars with high purity[1] (e.g. A. W.

★ E-mail: f.sestito@herts.ac.uk

[1]Purity is simply defined as the percentage of those stars that are confirmed to be members over the total number of candidates.

McConnachie & K. A. Venn 2020; G. Battaglia et al. 2022; A. B. Pace, D. Erkal & T. S. Li 2022; Y. Qi et al. 2022; J. Jensen et al. 2024), even in the extreme outskirts of galaxies (up to ∼12 half-light radii, e.g. A. Chiti et al. 2021; C. Filion & R. F. G. Wyse 2021; N. Longeard et al. 2022, 2023, 2025; Y. Yang et al. 2022; S. Vitali et al. 2022; C. R. Hayes et al. 2023; I. U. Roederer et al. 2023; F. Sestito et al. 2023b, c, 2024a, b; S. E. T. Smith et al. 2023; F. Waller et al. 2023; E. A. Tau, A. K. Vivas & C. E. Martínez-Vázquez 2024; K. S. Sato et al. 2025).

The relatively small sizes and low masses of dwarf galaxies make them extremely susceptible to not only internal but also external physical processes that determine their morphologies, especially in their outskirts (e.g. C. R. Higgs et al. 2021, and references therein). Among the internal processes, those that can influence the morphologies are star formation and stellar feedback (e.g. K. El-Badry et al. 2018); the external processes include mergers (e.g. A. J. Deason et al. 2022), ram pressure stirring (e.g. S. Kazantzidis et al. 2011) and stripping (e.g. E. K. Grebel, J. S. III Gallagher & D. Harbeck 2003), tidal interaction (e.g. J. Peñarrubia, J. F. Navarro & A. W. McConnachie 2008; A. Fattahi et al. 2018), and reionization (e.g. C. Wheeler et al. 2019). Therefore, studying the chemodynamical properties of individual stars from the inner regions to the extreme outskirts of a dwarf galaxy is crucial to understand these physical processes that drive galaxy formation and evolution.

To confirm the membership, radial velocities are need to remove foreground and background stars. While *Gaia*'s RV is too shallow, multi-object spectrographs (MOS) with thousands of fibres will drastically improve our knowledge on dwarf galaxies, e.g. WEAVE (G. Dalton et al. 2012; S. Jin et al. 2024), 4MOST (T. Bensby et al. 2019; Á. Skúladóttir et al. 2023), and PFS (N. Tamura et al. 2016; M. Chiba et al. 2026).

The MOS survey we use here is the Dark Energy Spectroscopic Instrument data release 1 (DESI DR1), which has the primary goal to investigate the nature of the dark energy and the expansion of the Universe (e.g. DESI Collaboration 2016, 2024; C. Poppett et al. 2024). The second goal of DESI, under bright observing conditions, is to observe stars in the Local Group, using its 5000 fibres (S. E. Koposov et al. 2024; S. Koposov et al. 2026; A. P. Cooper et al. 2023).

So far radial velocities and metallicities from DESI DR1 (S. Koposov et al. 2026; A. P. Cooper et al. 2023) have been used to study the properties of five stellar structures in the Milky Way halo (B. Kim et al. 2025); to derive the metallicity gradient, the velocity and its dispersion of Draco dwarf galaxy (J. Ding et al. 2025); and to investigate the astrophysical J and D factors in Sextans, Draco, and Ursa Minor using stars within 2.5 half-light radii (in addition to private DESI data, H. Yang et al. 2025).

In this paper, we use radial velocities and metallicities from the full data set of DESI DR1 to confirm or rejects DGs candidate members from G. Battaglia et al. (2022), and A. B. Pace et al. (2022). Section 2 describes the data used in this work; Section 3 reports the selection criteria adopted to confirm membership of DESI targets; Section 4 describes the galaxies with at least one star observed by DESI DR1. Section 5 focuses on the Sextans dwarf galaxy, as it is the second-most galaxy with the highest number of members observed by DESI DR1, and for which we are identifying new members in its extreme outskirts (up to ∼10 half-light radii). The chemodynamical properties of Sextans using DESI DR1 data are discussed, also with respect the literature, and compared to novel galactic chemical evolution models and cosmological hydrodynamical zoom-in simulations. Section 6 focuses on the most metal-poor star candidates related to the systems discussed in this paper; lastly, Section 7 summarizes our work.

2 DATA

In this work, we use metallicities and radial velocities from the DESI DR1 stellar catalogue[2] (S. Koposov et al. 2026), from which we use the DESI quantities extracted with the SP pipeline (A. P. Cooper et al. 2023), to confirm stellar members in Local Group galaxies. The pipeline uses a code based on FERRE[3] (C. Allende Prieto et al. 2006). DESI DR1 metallicities [Fe/H] have been corrected by the offset described in S. Koposov et al. (2026, see their table 4 and equation 2), using a second-order polynomial relation between the uncalibrated [Fe/H] and the derived effective temperature of the star[4]. Uncertainties on the radial velocities have been increased, adding a 0.9 km s^{-1} in quadrature (S. Koposov et al. 2026).

The DESI DR1 pipeline (B. Kim et al. 2025) also extracts elemental abundances for carbon, for some α-elements (Ca, Mg, Si, Na, Al, and a general α), and for Fe-peak elements (Fe, Cr, Ni, and Ti). However, S. Koposov et al. (2026) concluded that only the elemental abundances of Mg, Ca, and Fe are reliable. In addition, DESI DR1 elemental abundances show a strong anticorrelation with metallicities, especially at the low-metallicity ends (see fig. 6 of S. Koposov et al. 2026). In this work, we explore DESI DR1 elemental abundances of α-elements ([α, Mg, Ca/Fe]) for the Sextans dwarf galaxy only, and we compare them with high-resolution spectroscopic values from the literature and galactic chemical evolution models.

3 SELECTION CRITERIA OF THE DWARF GALAXY MEMBERS

First of all, cross-matched with *Gaia* DR3, DESI DR1 data are filtered using the following criteria (selection 1):

(i) *Gaia*'s parallax $\varpi < 0.1$ mas in order to remove the majority of Milky Way stars.

(ii) Position within 10 half light-radii (r_h) from the centre of a given system, not to cut out any potential members in the extreme outskirts of systems (e.g. G. Battaglia et al. 2022; A. B. Pace et al. 2022; F. Sestito et al. 2023b, c; J. Jensen et al. 2024); values of the systems' r_h are taken from G. Battaglia et al. (2022).

(iii) DESI DR1's surface gravity $\log(g) < 4$ and BESTGRID != S_RDESI1 as a fit-quality cut discussed in S. Koposov et al. (2026). No further cut based on RR_SPECTYPE or RVS_WARN flags is used as they are not included in the SP pipeline.

(iv) To avoid background galaxies as discussed in M. Riello et al. (2021), imposing GAIA_ASTROMETRIC_EXCESS_NOISE < 1 and GAIA_PHOT_BP_RP_EXCESS_FACTOR $< 1.3 + 0.06 \times (\mathrm{BP} - \mathrm{RP})^2$.

(v) Radial velocity uncertainties ≤ 15 km s^{-1}.

The second set of criteria restricts to stars if they align with an isochrone in the colour–magnitude diagram (CMD), and if they

[2]The mwsall-pix-iron.fits table is used in this work.

[3]The SP pipeline is preferred over the RVS, as we tested values from FERRE code against those from high-resolution spectroscopic (e.g. radial velocity, [Fe/H], surface gravity, and effective temperature) in various works (A. Arentsen et al. 2021; A. Ardern-Arentsen et al. 2024; D. S. Aguado et al. 2019; F. Sestito et al. 2023a, 2024a, b), finding good agreement.

[4]This correction is not applied to hot stars, i.e. all stars in M33 and IC1613.

move, in proper motion and line of sight velocity, similarly as the system (selection 2). More specifically, we select stars:

(i) within 0.2 mag in colour (BP – RP), which is well beyond the uncertainties on the *Gaia* colour, and 2σ from the distance modulus error in G mag. A very metal-poor ([Fe/H] $= -2.0$) PARSEC isochrone (A. Bressan et al. 2012) with stellar age of 10 Gyr is used in this work;
(ii) proper motion within $1.5\,\mathrm{mas\,yr^{-1}}$ of the systemic motion (values from G. Battaglia et al. 2022), i.e. $|\mathrm{ppm} - \mathrm{ppm_{system}}| - \sigma_{\mathrm{ppm}} \leq 1.5\ \mathrm{mas\ yr^{-1}}$; and
(iii) line-of-sight velocities around the mean systemic velocity (values from G. Battaglia et al. 2022; A. W. McConnachie & K. A. Venn 2020) and within 5 times of its velocity dispersion, i.e. $|\mathrm{RV} - \mathrm{RV_{system}}| <= 5 \times \sigma_{\mathrm{RV,sys}} + \sigma_{\mathrm{RV}}$.

Finally (selection 3), stars that passed the above two sets of selection criteria are cross-matched with the candidate member catalogues from G. Battaglia et al. (2022, hereafter B22) and A. B. Pace et al. (2022, hereafter P22), imposing a probability to be a member > 50 per cent from their Bayesian algorithms. The algorithms from B22 or P22 assign a probability to be a member of a given system based on the position on the sky, CMD, and proper motion.[5] Stars from our selection have a mean uncertainty on the DESI radial velocities of ~ 3.3 km s^{-1}, while the mean uncertainty on the metallicity is ~ 0.4 dex.

4 GALAXIES IN DESI DR1

We identified 15 systems from the cross-matching B22 and P22 with DESI DR1 data, including ultra-faint dwarfs (e.g. Hercules, Coma Berenice), classical dwarf galaxies (e.g. Sextans, Draco), a spiral galaxy (M33) and an irregular dwarf galaxy (IC1613). Each row of panels in Fig. 1 shows the projected position on the sky in the direction of a given galaxy for which we identified at least one member (first panel), the *Gaia* colour–magnitude diagram (second), the proper motion space (third), and the metallicity versus radial velocity for DESI DR1 stars (fourth).

In the figure, blue small crosses are stars that passed only our selection 1 and thus should be considered as contaminant stars, as their CMD positions, their proper motions, and/or their radial velocities likely offset from those of the system[6]. Black filled circles are those stars that pass our selections 1+2 but are not present in either B22 or P22, and thus new members. Red and blue circles are those stars passing selection 1+2+3 from B22 and P22 catalogue, respectively, and are confirmed members. Interestingly, when present, new members (black circles) are located more outwardly than those members from B22 and P22. This can be explained by the fact that *Gaia*-only based algorithms might have missed some members in such outskirts of galaxies. These outskirts members can be recovered once spectroscopic information (RV at least) are used as in this paper.

In addition, red and blue rhombus are stars that were likely candidate members (probability > 50 per cent) according to B22 or P22, respectively, but their DESI DR1 velocity is not compatible with the system's one within 5 times its velocity dispersion. Moreover, known member stars from the Stellar Abundances for Galactic Archaeology Database (SAGA; T. Suda et al. 2008) have been added as a reference in the first and fourth panels (dark green squares). Table 1 reports the number of new members, those confirmed or rejected candidates from B22 and P22, as well as the stellar masses of the galaxies studied in this work. In the following subsections, we report the candidate members for each of the systems observed in DESI DR1. The full list of these targets and their IDs will be provided as online material only.

So far, there are only two works that used DESI DR1 in addition to other data to investigate dwarf galaxies in the Local Group. J. Ding et al. (2025) focused on Draco only, while H. Yang et al. (2025) investigated the dark matter properties in Draco, Sextans and Ursa Minor. While these works mostly use candidate members from P22, we also use the larger list from B22. Note that while H. Yang et al. (2025) reports the finding of 1003 members in Ursa Minor, adopting the list of P22, we find none. This discrepancy is caused by the fact that H. Yang et al. (2025) used DESI tertiary data that are not part of the DR1 or of the science verification, and are not currently available.

4.1 Bootes II

There is only one candidate member form B22 that has been observed by DESI DR1 and we confirm its membership given its radial velocity (RV). Recently, N. Longeard et al. (2025) confirmed the membership of 9 candidates in Bootes II, using FLAMES spectrograph, 8 of which had a high membership probability in B22. However, only one star is in DESI DR1, which is the red circle in Fig. 1.

4.2 Bootes III

There are 4 confirmed members from B22, one of which is also in P22. In addition, there are 3 stars that are not likely members in either B22 or P22, but are found to be confirmed members, given their DESI DR1 RVs.

4.3 Canes Venatici I

There are 14 stars from B22 confirmed to be members of Canes Venatici I, including only one from P22; the rest of the candidates in P22 have a very low probability to be members.

4.4 Canes Venatici II

Three likely candidate members from B22 are confirmed to be members with DESI DR1 RVs.

4.5 Coma Berenice

All the 5 likely candidate members, that are in both B22 and P22, are confirmed to be members.

4.6 DES J0225+0304

DES J0225+0304 is a system, which is associated with the Sagittarius stellar stream, and, so far, there is no estimate for its

[5] In addition to those quantities and only for some systems, B22 also uses spectroscopic information. However, differences in membership estimation are minor and not relevant for the scope of this work. For P22, the MEM_FIXED probability is chosen.
[6] Those contaminant stars close to the CMD have RVs or proper motions that differ consistently from the systemic values, given the selection criteria.

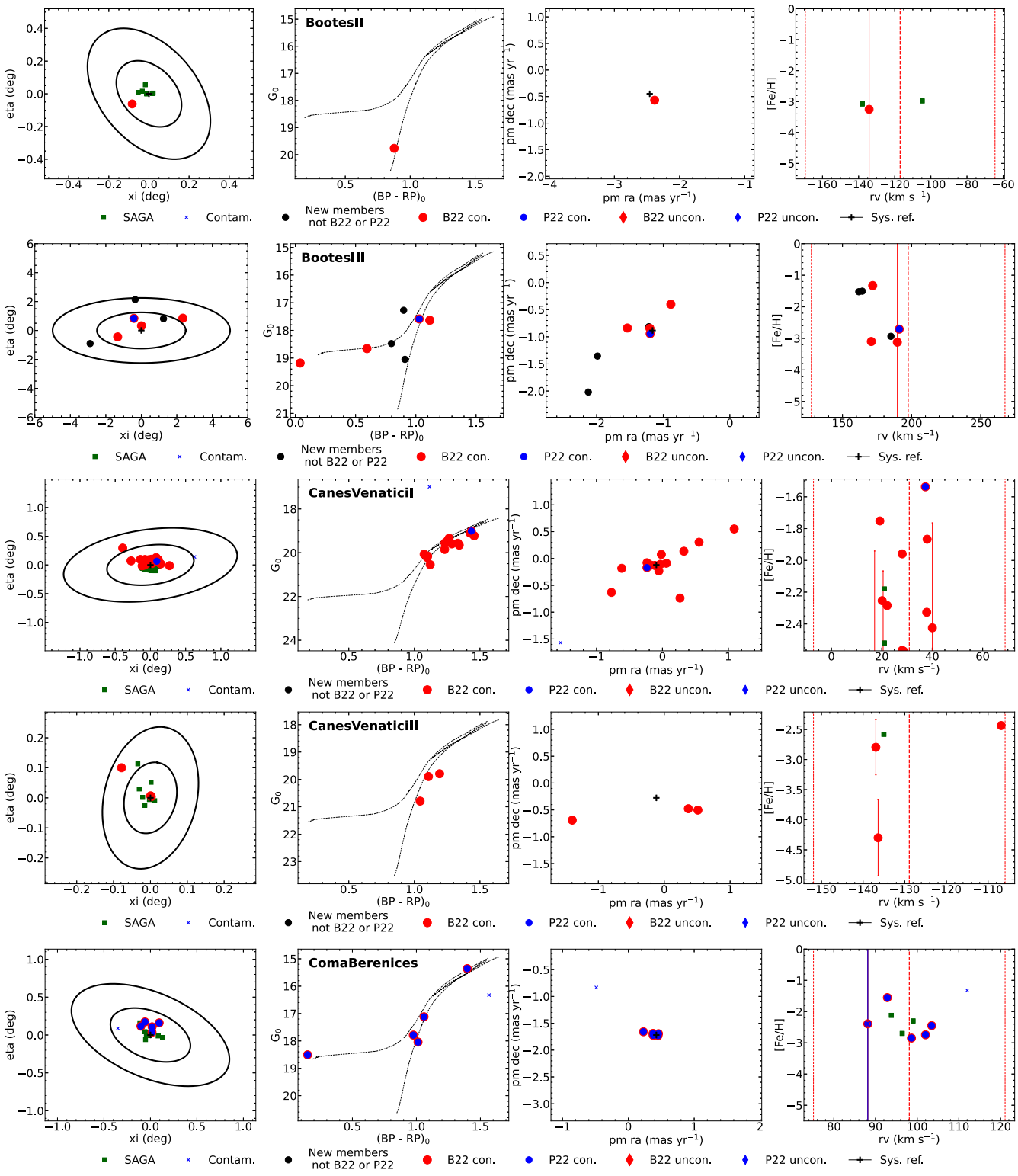

Figure 1. Properties of the Local Group galaxies seen in DESI DR1. Fist column: projected on sky position. Two black ellipses represent 5 and 10 half-light radii. Black plus markers denote the position of the system's centre. Second column: *Gaia*'s *colour–magnitude* diagram. An old (10 Gyr) very metal-poor ([Fe/H] = −2.0) PARSEC isochrone (A. Bressan et al. 2012) is represented with a black dotted line. Third column: *Gaia* proper motion space. Black plus markers denote the systemic proper motion. Forth column: metallicity versus radial velocity space. The three vertical dashed-lines denote the systemic line-of-sight velocity ±5 times its velocity dispersion.

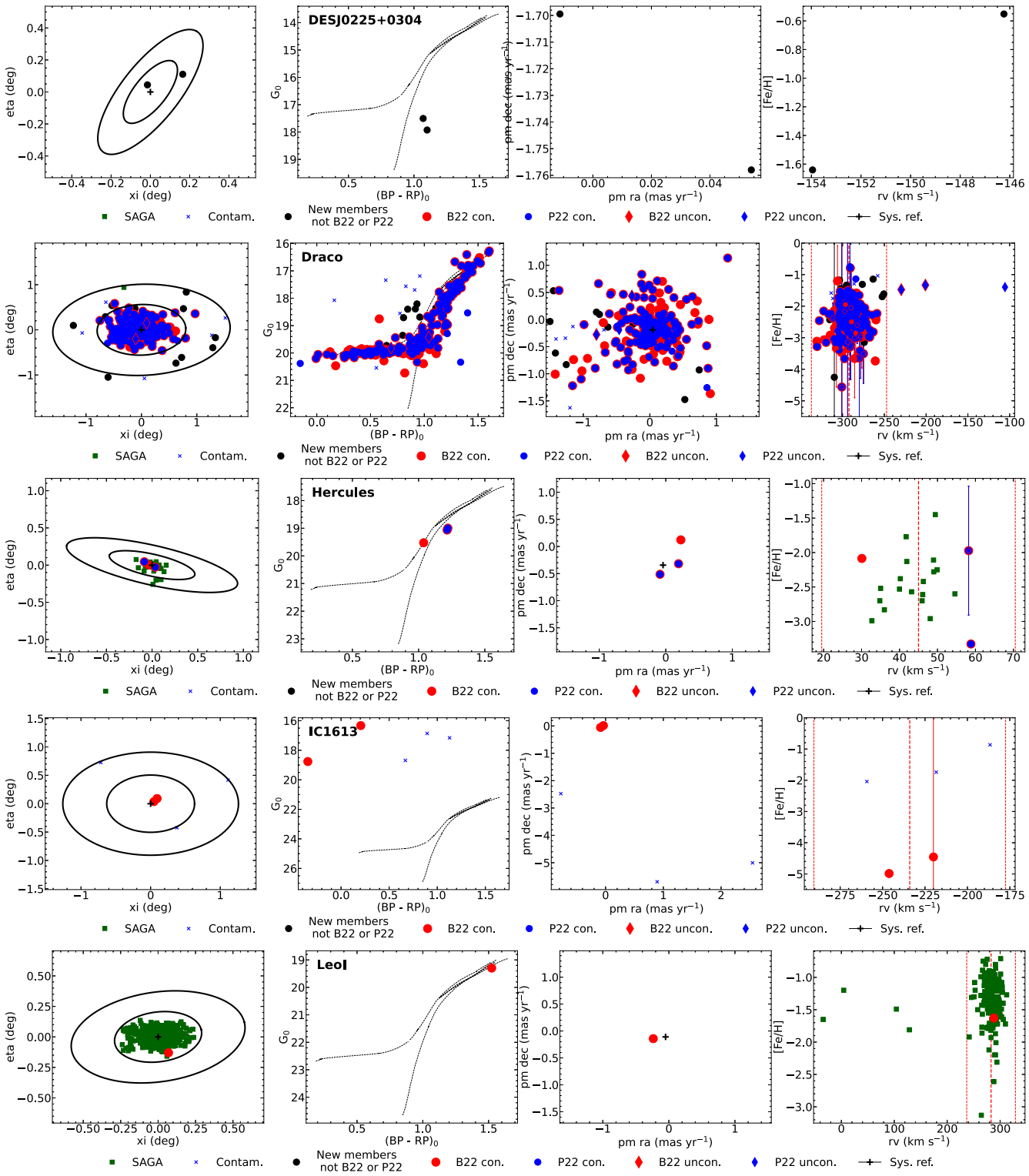

Figure 1. (continued) Properties of the Local Group galaxies seen in DESI DR1.

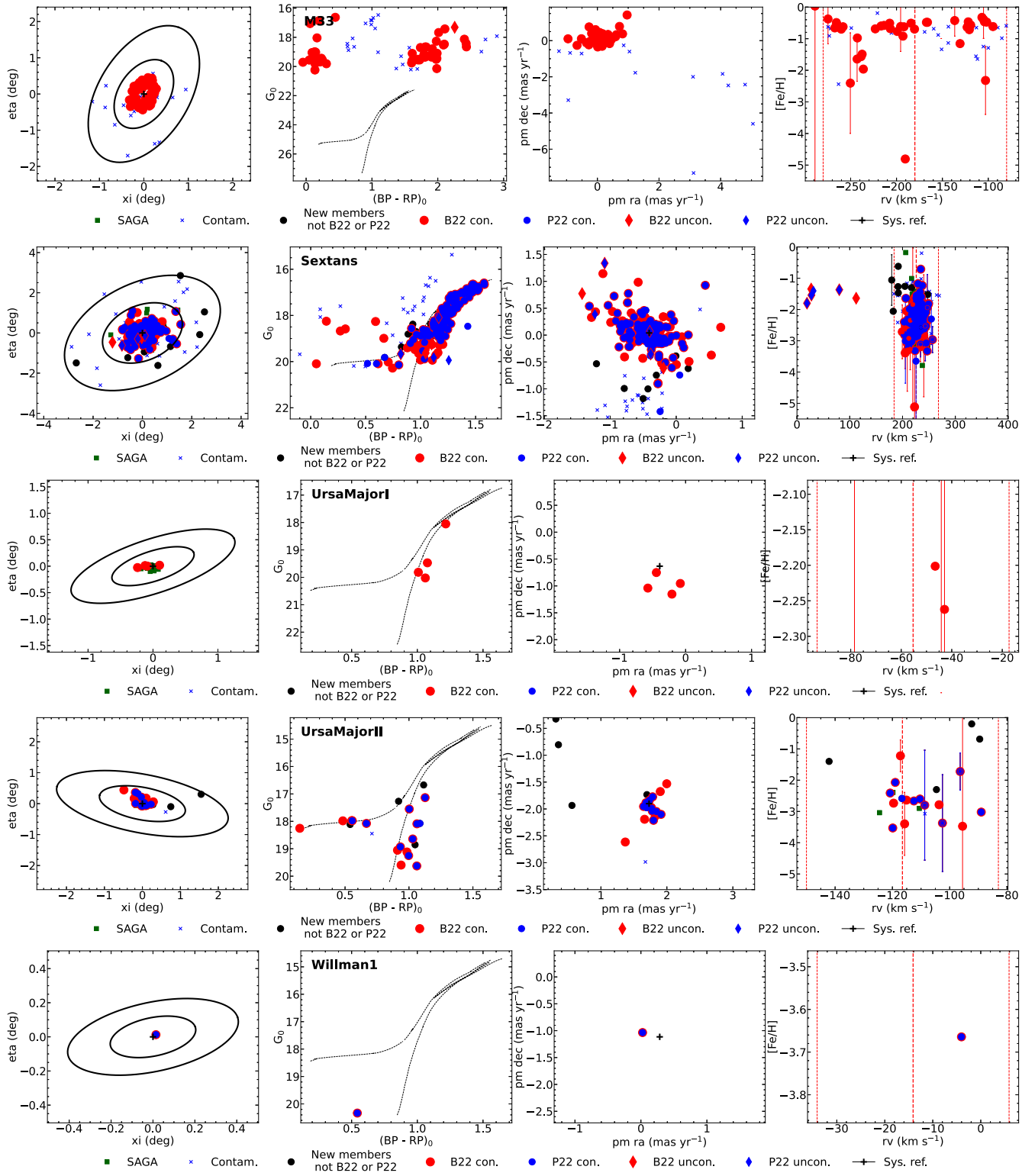

Figure 1. (continued) Properties of the Local Group galaxies seen in DESI DR1.

systemic radial velocity (e.g. E. Luque et al. 2017). Recently, A. W. McConnachie & K. A. Venn (2020) derived the systemic proper motion using *Gaia* EDR3.

We find two stars, in the direction of DES J0225+0304, observed by DESI DR1, which are not in the catalogues of B22 nor P22. These stars have similar proper motions and DESI DR1 radial velocities. Their proper motion values are within $\sim 1.8\sigma$ and $\sim 1.5\sigma$ from the systemic values in right ascension and declination reported by A. W. McConnachie & K. A. Venn (2020), respectively. If these stars are truly members of DES J0225+0304, then we obtain, for the first time, a systemic radial velocity of $\mathrm{RV_{sys}} = -150.0 \pm 7.0\ \mathrm{km\ s^{-1}}$.

Table 1. Number of confirmed and rejected members for each identified galaxy, cross-matching DESI DR1 with the candidates in B22 and P22. Stellar masses are from A. W. McConnachie (2012, and references therein), with the exception of M33 (R. P. van der Marel et al. 2012). BootesIII is strongly influenced by tidal forces and no stellar mass value is available (J. L. Carlin & D. J. Sand 2018).

Galaxy	$M_\star$ (10^4 $M_\odot$)	New members not in B22 nor P22	Confirmed B22	Confirmed P22	Confirmed B22 and P22	Unconfirmed B22	Unconfirmed P22	Unconfirmed B22 and P22
BootesII	0.1	0	1	0	0	0	0	0
BootesIII	Tidally disrupted	3	4	1	1	0	0	0
CanesVenaticiI	23	0	14	1	1	0	0	0
CanesVenaticiII	0.79	0	3	0	0	0	0	0
ComaBerenices	0.37	0	5	5	5	0	0	0
DES J0225+0304	N/A	2	0	0	0	0	0	0
Draco	29	12	212	161	157	2	3	2
Hercules	3.7	0	3	2	2	0	0	0
IC1613	10,000	0	2	0	0	0	0	0
LeoI	550	0	1	0	0	0	0	0
M33	300,000	0	49	0	0	1	0	0
Sextans	44	9	144	117	110	5	4	3
UrsaMajorI	1.4	0	4	0	0	0	0	0
UrsaMajorII	0.41	4	15	10	9	0	0	0
Willman1	0.1	0	1	1	1	0	0	0

4.7 Draco

We confirm 212 and 161 stars from B22 and P22, respectively, with 157 in common, to be members of Draco. On the other hand, we reject 2 and 3 stars from the two catalogues (B22 and P22, respectively), out of which 2 candidates are in common. Given the DESI DR1 RVs, we add 12 more member stars to Draco.

Recently, the DESI DR1 view of Draco was also discussed in J. Ding et al. (2025). Their work identified 155 members using astrometry, radial velocities and metallicities. They found 8 stars located outside the tidal radius (Stars 1–8 in their table 3). With our membership selection (see the criteria $1+2+3$ in Section 3), either using B22 or P22, we confirm the membership of 5 out of the 8 extra-tidal stars. Moreover, applying our selection criteria $1+2$, we can recover 11 stars that were neither in B22 nor P22. Only one of these was found to be an extra-tidal star in J. Ding et al. (2025). Therefore, we can identify more extra-tidal stars combining all the selection criteria, including 6 out of the 8 extra-tidal stars in J. Ding et al. (2025).

J. Ding et al. (2025) also derived the Draco's mean line of sight velocity, the velocity dispersion and the mean metallicity of the system, finding values compatible with previous attempts (E. N. Kirby et al. 2011, 2013; R. R. Muñoz et al. 2018). In addition, the metallicity gradient is steeper within the first half-light radius, while it flattens in the outskirts of the system (J. Ding et al. 2025).

4.8 Hercules

Three candidate members from B22 are confirmed to be members. Two of them are also present in P22. N. Longeard et al. (2023) identified 3 new members using the AAOmega spectrograph. None of these stars are present in B22, P22, nor in DESI DR1.

4.9 IC1613

IC1613 is an irregular dwarf galaxy, that includes RR Lyrae variable stars and Wolf–Rayet stars, and thus it is not possible to fit its CMD with an old isochrone, as discussed bs B22. Therefore, they did not apply the CMD selection, neither do we. We confirm the membership of the two B22 candidate members, given their RVs.

4.10 Leo I

The only B22 candidate member is confirmed to be a member, given its DESI DR1 RV.

4.11 M33

Similarly to IC1613, M33 hosts young stars and, as discussed in B22, the CMD cannot be used to select candidate members. We confirm 49 members from B22, while stars are rejected given their RVs.

4.12 Sextans

We confirm 144 and 117 stars from B22 and P22, respectively, with 110 in common, to be members of Sextans. On the other hand, we reject 5 and 4 stars from the two catalogues (B22 and P22, respectively), out of which 3 rejected candidates are in common. Given the DESI DR1 RVs, we add 9 more member stars to Sextans. DESI DR1 data have also been recently used by H. Yang et al. (2025) to investigate the astrophysical J and D factors in Sextans. They found 240 Sextans members starting from the P22 candidates list. This number is double than our selection from P22 or from B22. However, we note that, while H. Yang et al. (2025) remove stars with half-light radius $> 2.5\ r_{\rm h}$, we are able to find new members out to $\sim 10\ r_{\rm h}$.

4.13 Ursa Major I

4 candidate members from B22 are confirmed to be members, given their RVs from DESI DR1.

4.14 Ursa Major II

9 stars are candidate members from both B22 and P22, all of them are confirmed members. In addition to that, 6 stars from B22 and

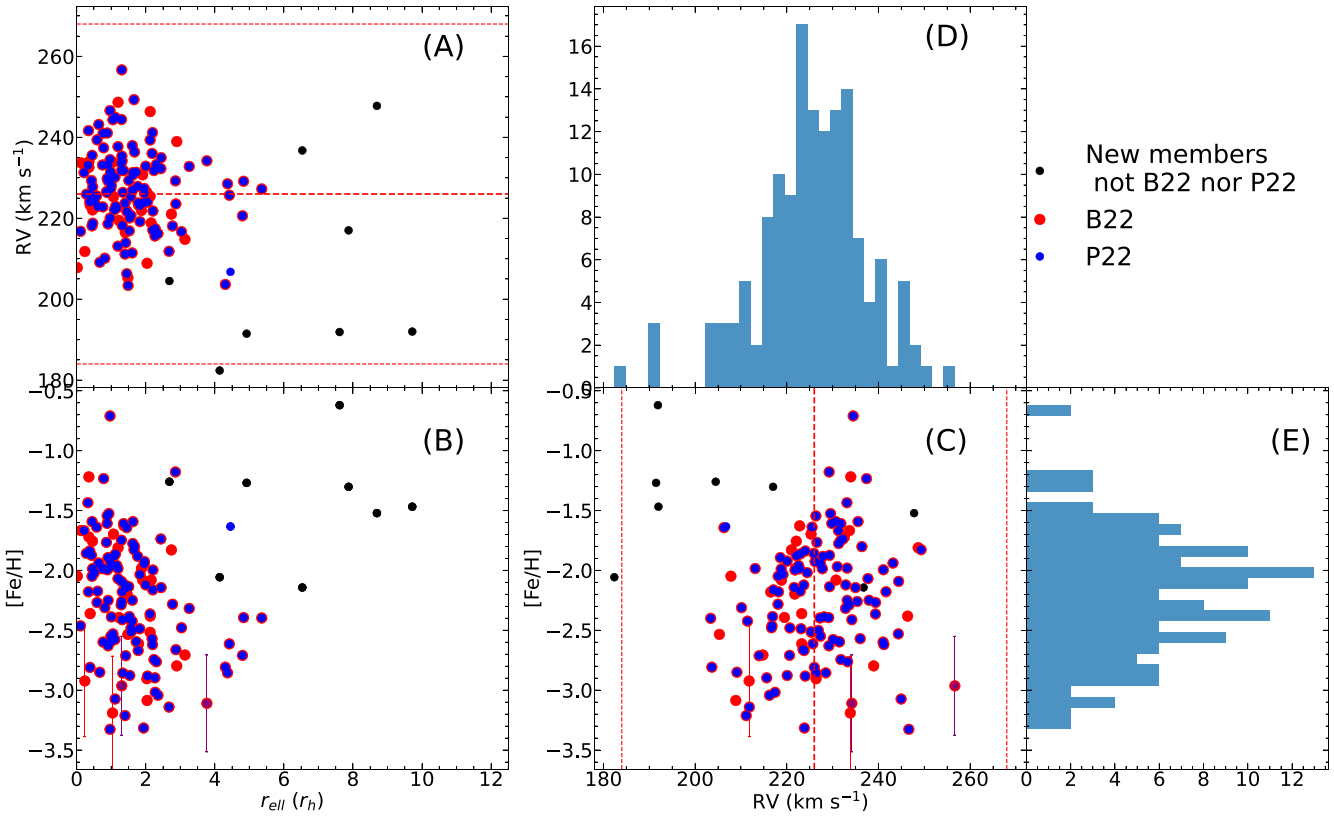

Figure 2. Radial velocities and metallicities in Sextans. Panel (A): RVs as a function of the projected elliptical distance. Panel (B): [Fe/H] as a function of the projected elliptical distance. Panel (C): [Fe/H] versus RVs. Panel (D): RVs' histogram. Panel (E): metallicities' histogram. Stars with large uncertainties on the metallicities, $\sigma_{[Fe/H]} > 1.0$ dex, have been removed. Stars with $\sigma_{[Fe/H]} > 0.5$ dex are shown with error bars.

one from P22 are confirmed to be members. 4 stars do not pass the probability cuts from those catalogues; however, their radial velocities are in agreement with those of Ursa Major II therefore likely to be members.

4.15 Willman I

The only candidate member, which is present in both B22 and P22 catalogues, is confirmed to be a member.

4.16 *Gaia* candidate membership success

There are various *Gaia*-based algorithms in the literature to provide a probability to be a member of a given system (e.g. A. W. McConnachie & K. A. Venn 2020; G. Battaglia et al. 2022; A. B. Pace et al. 2022; Y. Qi et al. 2022; J. Jensen et al. 2024). Given the chosen membership probability threshold in this work, we find a purity of $\gtrsim$ 96 per cent (see Table 1). Therefore, algorithms based on the exquisite *Gaia* data are able to provide high-purity membership, which can also be increased if stricter cuts on the probability are applied, although reducing the completeness and size of the sample.

We note that, for most of the systems studied in this work, the algorithm from B22 provides a higher number of candidates than those from P22, when adopting the same cut on probability. We want to stress out that different algorithms might have a different efficiency to weed out the foreground contamination, as well as a different optimisation for reaching the outskirts of the systems. Confirmation with ground-based MOS is crucial to explore the halo of dwarf galaxies, especially their outskirts.

5 CHEMODYNAMICAL PROPERTIES OF SEXTANS

In this section, we focus on the chemodynamical properties of Sextans, which is the galaxy with the largest number of new members after Draco, which is already studied in other works (J. Ding et al. 2025). DESI radial velocities and metallicities are used to derive the line-of-sight systemic velocity, the velocity dispersion, and the metallicity gradient of Sextans, while DESI elemental abundances for $\alpha-$elements in Sextans are compared with high-resolution spectroscopic data from the literature, our galactic chemical evolution models (e.g. C. Kobayashi et al. 2020a), and our chemodynamical simulations (e.g. F. Vincenzo & C. Kobayashi 2020, Sestito et al., in preparation).

5.1 Systemic velocities and metallicities

Panels of Fig. 2 show the radial velocities (RVs) and metallicities ([Fe/H]) in Sextans for those member stars found in B22 (red circles), in P22 (blue circles), and in DESI alone (black circles), with uncertainty on metallicity $\sigma_{[Fe/H]} < 1.0$ dex. Panels A and B of Fig. 2 display RVs and [Fe/H] as a function of the projected elliptical distances, normalized by the half light radius ($r_h = 21.4$ arcmin, or ~ 0.7 kpc, B22). Panel (C) shows RV versus [Fe/H], while panels (D) and (E) represent the histograms on these two

Table 2. Systemic velocities, systemic mean metallicity, and their dispersion for the various samples. Addd values fromm k26 and B11.

Selection	Sample	Sample size	Systemic RV (km s^{-1})	Systemic σ_{RV} (km s^{-1})	Systemic [Fe/H] (dex)	Systemic $\sigma_{[Fe/H]}$ (dex)
B22 + P22 + New	All	160	$225.04^{+0.98}_{-0.98}$	$11.17^{+0.78}_{-0.72}$	$-2.20^{+0.04}_{-0.04}$	$0.48^{+0.03}_{-0.03}$
B22 + P22 + New	[Fe/H] < -2.0	102	$224.82^{+1.20}_{-1.20}$	$10.79^{+1.00}_{-0.89}$		
B22 + P22 + New	[Fe/H] > -2.0	58	$225.41^{+1.69}_{-1.69}$	$12.07^{+1.44}_{-1.24}$		
B22 + P22	All	151	$226.12^{+0.82}_{-0.84}$	$8.87^{+0.71}_{-0.63}$	$-2.24^{+0.04}_{-0.04}$	$0.45^{+0.03}_{-0.03}$
B22 + P22	[Fe/H] < -2.0	100	$225.16^{+1.11}_{-1.11}$	$9.69^{+0.94}_{-0.84}$		
B22 + P22	[Fe/H] > -2.0	51	$227.71^{+1.18}_{-1.18}$	$7.45^{+1.05}_{-0.90}$		
S. Koposov et al. (2026)					$-2.24^{+0.03}_{-0.04}$	$0.44^{+0.03}_{-0.03}$
G. Battaglia et al. (2022)			226.0 ± 0.6	8.4 ± 0.4	-1.90 ± 0.01	0.6

quantities. In panels (B) and (C), stars with $\sigma_{[Fe/H]} \geq 0.5$ dex are shown with their error bars.

Table 2 reports the systemic line-of-sight velocity, the systemic mean metallicity and their systemic dispersions. These value are derived with a Markov chain Monte Carlo, based on the Metropolis–Hastings algorithm (W. K. Hastings 1970), similarly to what adopted by N. Longeard et al. (2020). As this is embedded in a Bayesian framework, the adopted prior is simply a step function of the expected radial velocities ($150 < RV < 300$ km s^{-1}), of the velocity dispersion ($\sigma_{RV} < 30$ km s^{-1}), of the expected mean metallicity ($-5 \leq$ [Fe/H] ≤ -1), and of the metallicity dispersion ($\sigma_{[Fe/H]} < 0.5$ dex). The likelihood is a Gaussian distribution, which is centred on the systemic RV (or mean [Fe/H]), and with a dispersion equal to the sum in quadrature of the intrinsic dispersion of systemic RV (or mean [Fe/H]) and the uncertainties on the stellar RVs (or [Fe/H]).

Table 2 lists two sets of values: one using member stars from B22 plus P22 [B22 + P22], and another also including our new members from DESI alone [B22 + P22 + New]. For the [B22 + P22] sample, the derived systemic mean metallicity and its uncertainty are identical to those reported by the DESI DR1 stellar catalogue (table 7 of S. Koposov et al. 2026). The systemic metallicity dispersion is also in agreement within $\sim 0.24\,\sigma$ from the value in S. Koposov et al. (2026). Adding our new members, for the [B22 + P22 + New] sample, our systemic mean metallicity and its dispersion are still in *agreement* within $0.80\,\sigma$ and $0.94\,\sigma$ from S. Koposov et al. (2026), respectively.

The systemic RV and its dispersion are also derived splitting the members according to their metallicities: the very metal-poor (VMP) group with [Fe/H] < -2.0 and the metal-rich (MR) with [Fe/H] > -2.0. This value for the threshold has been chosen to arbitrary divide those stars polluted by only Type II supernova from those in which Type Ia supernovae are also contributing (e.g R. Theler et al. 2020).

The systemic velocity and the velocity dispersion obtained in this work, either for all three sources [B22 + P22 + New] or only two sources [B22 + P22], are in agreement with the literature values from G. Battaglia et al. (2011). We notice that the B22 + P22 values are closer to those from G. Battaglia et al. (2011) than the other sample that includes also black circles (New).

Similar systemic radial velocities, i.e. within 1σ, are also obtained for the VMP and the MR stars, separately. For the velocity dispersion, we note and interesting trend; the MR σ_{RV} for [B22 + P22 + New] is larger than the VMP value, although we find the opposite behaviour for [B22 + P22]. As a result, the two VMP values from the different datasets are compatible within 1σ, while σ_{RV} differs only for the MR stars. The discrepancy between the two datasets (B22 + P22 + New versus B22 + P22) for the MR stars might be driven by some relatively metal-rich stars ($-1.5 \lesssim$ [Fe/H] $\lesssim -0.5$) that are also located in the outskirts of Sextans, all of them are New (black circles), hence they are not in B22 nor in P22 data sets. Curiously, there are only 8 member stars[7] newly identified by DESI (black circles) and almost half of them appear to be related to the dispersion velocity discrepancy.

5.2 Velocity and metallicity profiles: comparison with observations

The two panels of Fig. 3 show the mean metallicity (top) and the velocity dispersion (bottom) as a function of the projected elliptical distance in Sextans. Here, we use [B22 + P22] only as most of the new members are located in much outer regions (black circles in Fig. 2). Each point represents the mean of one of the two quantities in a bin that is wide $1r_h$. In this plot, blue markers are the members from B22 and P22, while black and olive circles represent data from G. Battaglia et al. (2011) and E. Tolstoy et al. (2025), respectively. Another data set would be E. N. Kirby et al. (2010); however, it is not included in this work as their observed Sextans stars are mostly locate in the inner regions of the system.

Recently, E. Tolstoy et al. (2025) have re-analysed the Sextans stars from G. Battaglia et al. (2011), including members from M. G. Walker et al. (2023). They discussed the presence of a double-peak profile in the Sextans' metallicity distribution, respectively at [Fe/H] ~ -3.0 and [Fe/H] ~ -2.0. These two populations have slightly different velocity dispersions, with the stars at [Fe/H] ~ -3.0 being more kinematically hotter. Panel (E) of Fig. 2 does not show trace of a double-peak metallicity profile, given the limited number of stars at the lowest-metallicities. However, we clearly see the radial gradients.

While the outskirts is more metal-poor and the metallicity gradient flattens out, compatible with null variations. The velocity dispersion increases with the distance from Sextans' centre. Such behaviour is in agreement with the previous findings from G. Battaglia et al. (2011) – which has almost no members beyond $3r_h$ –, and with those from E. Tolstoy et al. (2025). The outermost

[7]One of the 9 new identified members does not pass the stricter cut on the metallicity uncertainties applied in this section.

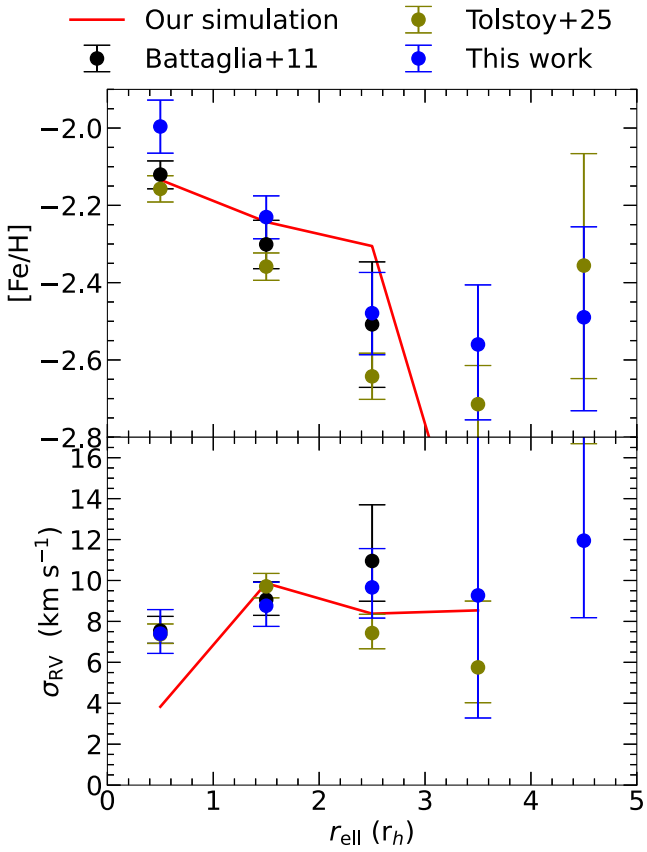

Figure 3. Mean metallicity (top) and velocity dispersion (bottom) as a function of the projected elliptical distance in Sextans (half-light radius units). Blue circles mark the median values calculated with the sample from B22 and P22. Black and olive circles represent the median values calculated with the samples from G. Battaglia et al. (2011) and E. Tolstoy et al. (2025), respectively. Red lines represent the values derived from our simulated dwarf satellite galaxy, with stellar mass of 4.6×10^5 $M_\odot$ (similar to Sextans, $\sim 4.4\times 10^5$ $M_\odot$), extracted from a cosmological 'zoom-in' hydrodynamical simulation of the Local Group (Sestito et al., in preparation). The mean metallicity of the simulated system has been shifted by +0.5 for a better visualisation of the data, while its shape remains intact. No shift has been applied to the velocity dispersion.

value of the velocity dispersion from E. Tolstoy et al. (2025) is out of the *y*-axis range as it is scarcely populated, providing not useful values compared to our DESI value.

5.3 Velocity and metallicity profiles: comparison with cosmological zoom-in simulations

The observed metallicity gradient and velocity dispersion profiles of Fig. 3 are also in great agreement with our simulated dwarf galaxy (red lines – a +0.5 dex has been added to the metallicity for a better visualization, without modifying its trend). The red lines represent the values derived from a Sextans-like dwarf satellite galaxy from our cosmological 'zoom-in' hydrodynamical simulation that also includes detailed chemical evolution (Sestito et al., in preparation); the simulation code is based on Gadget-3 (V. Springel 2005) including baryon physics described in C. Kobayashi, V. Springel & S. D. M. White (2007) and the latest nucleosynthesis yields from C. Kobayashi et al. (2020a) and C. Kobayashi, A. I. Karakas & M. Lugaro (2020b). The initial condition is taken from C. Scannapieco et al. (2012, Aq-C-4), which forms a Milky Way-type galaxy; the detailed properties of this main galaxy has been analysed in F. Vincenzo & C. Kobayashi (2020). The simulation also contains a few hundreds satellite galaxies, spanning a wide ranges of chemodynamical properties (Sestito et al., in preparation.), from which we selected an initial pool of 8 systems with stellar masses from $4–5 \times 10^5 M_\odot$, i.e. similar to Sextans' stellar mass. Half of the simulated dwarf galaxies experienced a merging event in their history, which have brought in approximately $\sim$ 8–13 per cent of their stellar masses. The other half of the sample has no accreted stars. The simulated galaxy that best matches the observed metallicity and velocity dispersion trends of Sextans has not experienced a merging event nor is tidally perturbed by other nearby systems. L. Cicuéndez & G. Battaglia (2018) suggested that Sextans might undergone an accretion event from the presence of a shell-like structure in the system north–east side, although the accreted mass was not estimated. The resolution of the AQ-C-4 suite does not permit to investigate accretion of systems with stellar masses $\lesssim 10^4$ $M_\odot$. As regard tidal perturbations, Sextans has a distant Galactic pericentre ($\sim$ 70 kpc), also far from the Magellanic clouds ($\gtrsim$ 100 kpc, G. Battaglia et al. 2022), and thus it is unlikely to be gravitationally perturbed by these more massive galaxies. Similarly, the simulated galaxy is far from other systems ($\gtrsim$ 100 kpc) at the present day. The stellar mass of the simulated galaxy is also very similar to that of Sextans, i.e. 4.6×10^5 $M_\odot$ (versus $\sim 4.4 \times 10^5$ $M_\odot$ for Sextans, G. Battaglia et al. 2022). On the star formation history, both the simulated galaxy and Sextans had one single episode of star formation. The simulated galaxy has formed half of its stellar content within $\sim$ 2.5 Gyr, which is comparable to the value reported by M. Bettinelli et al. (2018) for Sextans.

As we can see from Fig. 3, the inner region of Sextans has a higher mean metallicity, where also the metallicity gradient is steeper (~ -0.25 dex r_h^{-1} or $\sim -12 \times 10^{-3}$ dex arcmin^{-1} or ~ -0.36 dex kpc^{-1}).[8] In the outskirts ($r_h > 3$), the plot shows a constant metallicity value around ~ -2.5. The gradient in metallicity found with DESI DR1 data in this work is comparable with the values derived using the data from G. Battaglia et al. (2011) and E. Tolstoy et al. (2025), which are obtained from intermediate resolution spectroscopy of the VLT/FLAMES (R $\sim$ 6500). Recently, S. Taibi et al. (2022) discussed the metallicity gradient ranges in Local Group dwarf galaxies, using values from the literature. In S. Taibi et al. (2022), the reported value for Sextans' metallicity gradient is slightly steeper than those of other dwarf galaxies with similar luminosity, Galactic distance, stellar mass, gas mass, or star formation time-scale. The value we obtain from DESI DR1 data is consistent with that reported by S. Taibi et al. (2022) within $\sim 1\sigma$, but is slightly less steep, which makes Sextans' value closer to the 95 per cent confident interval obtained from all the Local Group DGs (see figs 3 and 4 of S. Taibi et al. 2022).

In relation to the formation of radial metallicity gradients, one could assume that the oldest and most metal-poor stars form everywhere in the systems; the enriched gas cools and sinks in the inner regions while part of it is expelled from the outskirts due to the lower potential; eventually, metal-rich stars form only in the inner regions (e.g. H.-X. Zhang et al. 2012; S. L. Hidalgo et al. 2013; A. Benítez-Llambay et al. 2016; Y. Revaz & P. Jablonka 2018). This mechanism, called 'outside-in' formation, is commonly observed among various Local Group dwarf galaxies (e.g.

[8] Assuming a half-light radius of 695 pc (A. W. McConnachie 2012) or of 21.4 arcmin (G. Battaglia et al. 2022).

G. Battaglia et al. 2011; M. G. Walker & J. Peñarrubia 2011; S. Vitali et al. 2022; E. Tolstoy et al. 2023; F. Sestito et al. 2023b, c, 2024b; J. M. Arroyo-Polonio et al. 2025; J. Ding et al. 2025). In addition, the recurrent star formation feedback might also push outwardly the oldest and most metal-poor stars from the centre. These will be investigated in our future work with our simulations.

In summary, Figs 2 and 3 show a metal-rich and kinematically colder population confined in the inner regions and a hotter, dispersed, more metal-poor one in the outskirts. The best way to distinguish these scenarios would be to derive detailed elemental abundances of stars.

5.4 Elemental abundances of the $\alpha-$elements

It has been shown that DESI DR1 elemental abundances [X/Fe] might present a strong anticorrelation with metallicities [Fe/H], especially for stars with the lowest metallicities (S. Koposov et al. 2026). None the less and with extreme caution, we show in Fig. 4 the [α/Fe] (top left panel), [Mg/Fe] (middle left panel), and [Ca/Fe] (bottom left panel), extracted by DESI DR1 pipeline (blue markers and grey error bars), as a function of [Fe/H], which show a significant scatter. For comparison, high-resolution spectroscopic values in local thermodynamic equilibrium (LTE, black circles) for 69 stars from L. Mashonkina et al. (2017, 2 stars), from R. Lucchesi et al. (2020, 2 stars), from W. Aoki et al. (2009, 6 stars) re-analysed in R. Lucchesi et al. (2020), from R. Theler et al. (2020, 38 stars), from I. U. Roederer et al. (2023, 5 stars), and from APOGEE DR17 (Abdurro'uf et al. 2022, 16 stars) are also plotted in the left panels. In the right panels, median values of the elemental abundances for both DESI DR1 (blue) and the literature (black) are are shown, which do not agree very well.

Elemental abundances expected from our galactic chemical evolution (GCE) model (red line) are plotted in the right column of Fig. 4. The GCE code is described in C. Kobayashi, T. Tsujimoto & K. Nomoto (2000), and the latest nucleosynthesis yields from C. Kobayashi et al. (2020a, 2020b) are included. For Type Ia supernovae (SNe Ia), both Chandrasekhar (Ch)-mass and sub-Ch mass explosions are included[9]. The model parameters of star formation, inflow, outflows are basically chosen for Sextans in C. Kobayashi et al. (2020a), but are revised to match the position of the $\alpha-$knee, which should appear at $-2.0 \lesssim$ [Fe/H] $\lesssim -1.5$ (R. Theler et al. 2020). More specifically, we increased (i) the time-scale for the star formation duration (from 100 to 200 Gyr), (ii) the time-scale for the outflow of gas (from 1.4 to 1.6 Gyr), and (iii) the contribution rate of sub-Ch SNe Ia by a factor of 1.5. The new version of the model is in excellent agreement with the high-resolution elemental abundances from the literature. To be noted, Mg has a steeper slope than Ca after the $\alpha-$knee ('the shin'), in both the GCE model and in the observed median [(Mg, Ca)/Fe] ratios. We interpret the different shin' slope as an evidence that sub-Ch SNe Ia contributed to the chemical evolution of Sextans, as this kind of SNe Ia produces more Ca than Mg (e.g. C. Kobayashi et al. 2020a).

For stars with [Fe/H] $\gtrsim -2.0$ (on the right of the vertical dashed grey line), there seems to be an agreement in the [α/Fe] and [Ca/Fe] between DESI DR1 and the high-resolution estimates, also between their median values within 1σ. [Mg/Fe] seems to be problematic as the distribution is more scattered in DESI. Literature data also show a trend, rather than a dispersion, in [(α, Mg, Ca)/Fe] at this metallicity regime. As also discussed in R. Theler et al. (2020), SNe Ia seem to start to contribute to the chemical enrichment of Sextans at these metallicities, which can explain the behaviour of the [X/Fe] from the literature. The slope at [Fe/H] $\gtrsim -2.0$ is shallower for Ca than Mg, which is also expected in the SN Ia nucleosynthesis (C. Kobayashi et al. 2020a). The position of the $\alpha-$knee at such [Fe/H] is similar to those of other DGs ($-2.5 \lesssim$ [Fe/H] $\lesssim -1.5$, e.g. E. Tolstoy et al. 2009; K. A. Venn et al. 2012; B. Hendricks et al. 2014; J. E. Norris et al. 2017; M. Reichert et al. 2020; R. Theler et al. 2020; F. Sestito et al. 2023c; S. Vitali et al. 2025). In DGs, the onset of SNe Ia happens at lower [Fe/H] than in the Milky Way, as the retention of metals in these relatively low-mass systems is less efficient than in the Galaxy (e.g. K. A. Venn et al. 2004; E. Tolstoy et al. 2009; M. Haywood et al. 2013; C. Kobayashi et al. 2020a).

For [Fe/H] $\lesssim -2.0$ (on the left of the vertical dashed grey line), DESI values show an unrealistic scatter in all the three left panels (up to ~ 1.5 dex for [Mg/Fe]). The extremely high or low values in [(α, Mg, Ca)/Fe] extracted by DESI DR1 in the very metal-poor regime are inconsistent with the GCE model and also the high-resolution literature data (except for 3 high-α stars, see more discussion in Appendix A). In addition, the median values of [X/Fe] increases as metallicity decreases (right panels), presenting a strong anticorrelation. The median values from DESI (blue circles) are systematically higher and with a steeper slope than the literature median values (black circles). The large scatter of [X/Fe] (especially for Mg), the numerous stars with extreme [X/Fe], and the strong anticorrelation with metallicity would imply extreme caution for any physical interpretation of the DESI elemental abundances at the lowest metallicities.

6 THE MOST METAL-POOR STARS

Ultra metal-poor (UMP, [Fe/H] < -4.0) stars are thought to be likely polluted by one supernova event originated by the First stars (e.g. A. Frebel & V. Bromm 2012; K. Nomoto, C. Kobayashi & N. Tominaga 2013; E. Starkenburg et al. 2018; T. Hartwig et al. 2023; P. Bonifacio et al. 2025). So far, less than 50 objects have been discovered in the Milky Way (F. Sestito et al. 2019; G. Limberg et al. 2025), and only three in dwarf galaxies, i.e. one in Sculptor (Á. Skúladóttir et al. 2021), one in the Large Magellanic Cloud (A. Chiti et al. 2024), and one in Pictor II (A. Chiti et al. 2026). As UMP stars are extremely rare objects (e.g. K. Youakim et al. 2017), the discovery new UMP stars in the Milky Way and its satellites would be invaluable for studying the chemical enrichment in the early Universe. Low-resolution spectroscopic surveys such as DESI can provide good candidates.

However, as spectral lines in UMP stars are very weak (e.g. E. Starkenburg et al. 2018; C. Lardo et al. 2021; Á. Skúladóttir et al. 2021; A. Chiti et al. 2024), automatic fitting pipelines of low-resolution spectra might not work properly on such objects, and thus we visually investigate the candidates as follows. In Figs 1 and 2, the most metal-poor stars are those possessing large uncertainties on the derived metallicities. We gather all the stars (members and unconfirmed members of systems studied in this work) in all galaxies to assemble a sample of candidate UMP stars with [Fe/H] $\lesssim -3.4$ (adding their uncertainty). We ease our selection criteria here from Section 3, including stars with

[9]Equation (2) of C. Kobayashi & K. Nomoto 2009 is used for both but with different secondary mass ranges; 0.835–1.9 $M_\odot$ for single degenerate systems (C. Kobayashi, K. Nomoto & I. Hachisu 2015) and 1.8–7.95$M_\odot$ for double degenerate systems, depending on the metallicity.

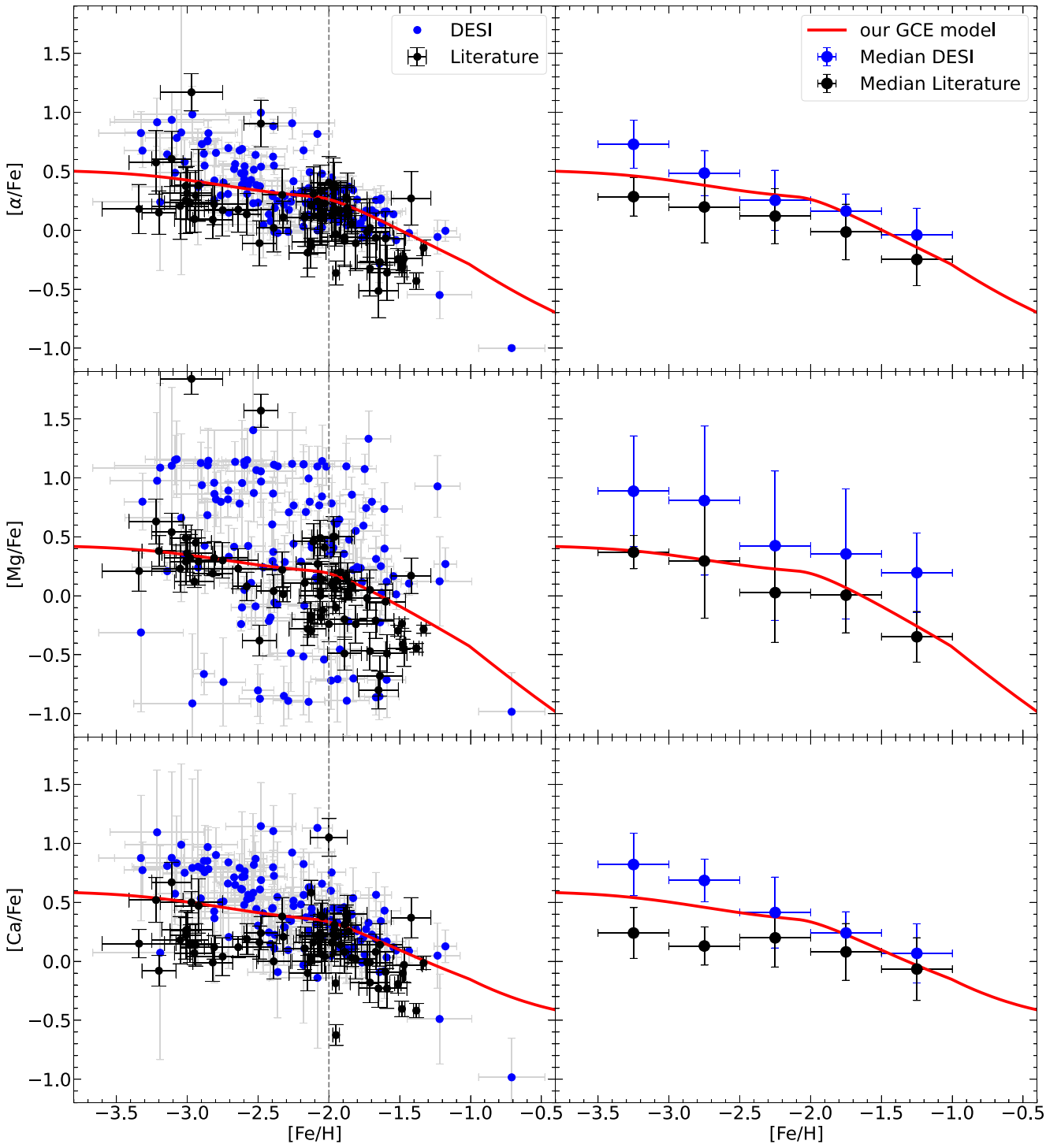

Figure 4. Elemental abundances of $\alpha-$elements in Sextans for [α/Fe] versus [Fe/H] (top), [Mg/Fe] versus [Fe/H] (middle), and [Ca/Fe] versus [Fe/H] (bottom). DESI DR1 and their median values are shown with blue + grey error bars (left panels) and blue circles (right panels), respectively. DESI stars with $\sigma_{[Fe/H]} > 0.5$ dex have been removed from the plot. Members stars are selected from B22 and P22. For comparison, black circles (left panels) are high-resolution spectroscopic LTE elemental abundances taken from L. Mashonkina et al. (2017); R. Lucchesi et al. (2020) with their revised sample from W. Aoki et al. (2009); R. Theler et al. (2020); I. U. Roederer et al. (2023), and from APOGEE DR17 (Abdurro'uf et al. 2022), while their median values are shown with black circles (right panels). Our GCE model for Sextans C. Kobayashi, S.-C. Leung & K. Nomoto (2020a) is also shown with a red line, which is revised to match the position of the $\alpha-$knee as in R. Theler et al. (2020). For the literature and gce model values, [α/Fe] is defined as the mean between [Ca/Fe] and [Mg/Fe], while for DESI data this quantity is extracted by the pipeline. APOGEE DR17 data are selected imposing SNR > 50, and on-sky position, radial velocities and proper motion compatible with those of Sextans. Error bars on the medians x-axis in the right panels denote the width of the bins. Vertical dashed grey lines mark the [Fe/H] at which, below that, DESI [X/Fe] are supposed to be 'not reliable'.

Table 3. Ultra metal-poor candidates in Local Group galaxies and contaminants. We report the DESI DR1 ID, the *Gaia* DR3 designation, the calibrated metallicity and its uncertainty, the derived signal-to-noise (SNR) ratio around the Ca II Triplet, the best grid flag adopted by DESI pipeline, the catalogue from which the object has been confirmed or unconfirmed (unc) as a member, and a column reporting whether the object is a UMP candidate or something else.

Galaxy field	DESI DR1 ID	*Gaia* DR3 Source ID	$[Fe/H]_{cal}$ (dex)	SNR @Ca II T	BESTGRID	Catalogue	Note
CVen II	39632966095209928	1515697326013099904	-4.30 ± 0.63	6.8	!=S_RDESI1	B22	UMP candidate
Dra	39633362771515905	1433204237051138304	-3.74 ± 0.33	8.5	!=S_RDESI1	B22	UMP candidate
Dra	39633356299700349	1433055729967360128	-3.66 ± 0.24	7.3	!=S_RDESI1	B22/P22	UMP candidate
Dra	39633362771509683	1433203820439296640	-3.62 ± 0.02	14.6	=S_RDESI1	B22/P22	$[Fe/H]_{CaT} = -2.7 \pm 0.2$
Sex	39627745013008688	3829135422249251968	-4.80 ± 0.72	2.5	!=S_RDESI1	B22 unc	UMP candidate
Sex	39627738977404585	3829118379819009024	-4.26 ± 0.63	2.0	!=S_RDESI1	B22 unc	UMP candidate
Sex	2305843037739159875	3829058177262521216	-3.61 ± 0.10	1.2	=S_RDESI1	B22/P22	UMP candidate
Sex	39627738981597619	3829065358447854592	-3.61 ± 0.13	2.4	=S_RDESI1	B22	UMP candidate
Sex	39627763140789618	3831439204052083584	-3.58 ± 0.06	7.3	=S_RDESI1	B22	UMP candidate
IC1613	2851374429634560	2539072107188195584	-4.99 ± 0.05	1.6	!=S_RDESI1	B22	Hot star
M33	1152921504619431695	303363474380375936	-4.81 ± 0.08	5.0	!=S_RDESI1	B22	Hot star
CVen I	39632956167291660	1469959020983848704	-3.876 ± 0.002	6.2	=S_RDESI1	New	Galaxy
Dra	39633359554480798	1433139292851749888	-4.03 ± 0.08	2.3	=S_RDESI1	B22/P22 unc	Galaxy
Dra	39633356308088548	1432939220389369984	-4.11 ± 0.04	4.0	=S_RDESI1	P22 unc	Galaxy
Sex	39627732933414594	3828973931478853632	-3.98 ± 0.02	3.7	=S_RDESI1	B22/P22 unc	Galaxy
Sex	39627732937606255	3829067007715281536	-3.67 ± 0.11	9.3	=S_RDESI1	B22/P22 unc	Galaxy

uncertainties on metallicity $\sigma_{[Fe/H]} < 1.0$ and stars with BESTGRID = S_RDESI1, and removing the limit on the RV uncertainties. This allows us to find 16 objects, listed in Table 3. We then use the DESI retriever tool[10] to download the DESI spectra and the model fit of these 16 objects. Upon inspection of their spectra, 5 objects are found to be emission line galaxies, all of which have BESTGRID = S_RDESI1. Two objects located in M33 and IC1613 are hot stars (as discussed in B22); therefore, they cannot be considered as old UMP stars.

The remaining 9 objects are stars and we inspect their spectra and derive the signal-to-noise ratio (SNR) around the Ca II Triplet. Examples of the DESI spectra (blue lines) and their spectral fitting models (red lines) for one star in Canes Venatici II and one in Draco are reported in Fig. 5. The panels of Fig. 5 display the H α (top left panel of each star), the Mg I Triplet (top right), the Ca II Triplet regions (bottom row).

The star in Canes Venatici II (top panels of Fig. 5) has a barely detectable H α line, while the Mg I Triplet and the Ca II Triplet lines are buried in the noise. Three UMP candidates are in Draco, two of them with BESTGRID != S_RDESI1. These two stars have H α lines that are detectable and relatively well fitted by the models, while their Mg I Triplet and the Ca II Triplet lines are barely detectable if not washed away by the noise. The remaining star in Draco, which is shown in the bottom panels of Fig. 5, has an SNR sufficient to detect H α and Ca II Triplet lines. There are 5 UMP candidates towards Sextans, two of them with BESTGRID != S_RDESI1. Both of them have very poor SNR, i.e. $\sim$2.5 and $\sim$2.0, which make their spectral fitting very unreliable. These two stars are Sextans candidate members from B22 and they did not pass our previous selection due to their large RV uncertainty of $\sim$120 and $\sim$140 km s^{-1}, respectively. Their SNR is so low that only H α is detectable in one of them (DESI ID 39627745013008688). The spectra of the remaining three stars also have low SNR values, although H α and Ca II Triplet lines are detectable or barely detectable, while the Mg I Triplet is too weak compared to the noise.

[10] https://github.com/segasai/desi_retriever/

Ca II Triplet lines have been widely used as a proxy for metallicity in giant stars (e.g. T. E. Armandroff & G. S. Da Costa 1991; G. Battaglia et al. 2008; E. Starkenburg et al. 2010; R. Carrera et al. 2013; N. Longeard et al. 2023) when dealing with low- or medium-resolution spectra. However, a SNR of at least $\sim$15 is needed to reliably estimate metallicity from the Ca II Triplet in the most metal-poor stars, as recently suggested by E. Tolstoy et al. (2025). We find only one star in Draco that has a sufficient SNR close to this threshold.

Finally, we compare the DESI spectrum of this Draco UMP candidates with our synthetic spectra generated from MARCS stellar atmospheres models (B. Gustafsson et al. 2008), assuming [Ca/Fe] = +0.4 (in line with the expected trend for α-elements, e.g. C. Kobayashi et al. 2020b) and adopting the stellar parameters from DESI DR1. Fig. 6 shows its normalized DESI spectrum (blue line), comparing to the synthetic spectra with [Fe/H] = -4.0, -3.0, and -2.0 (olive, red, and black dashed lines, respectively). The first two components of the Ca II Triplet are narrower than the synthetic model with [Fe/H] ~ -2.0, which might indicate a metallicity in the range $-3.0 \lesssim$ [Fe/H] $\lesssim -2.0$. The third Ca II Triplet line is too noisy for a fair comparison. In addition, the equivalent widths (EW) of the first two Ca II Triplet components have been measured (257 and 956 mÅ, respectively) to then estimate the [Fe/H], adopting the polynomial relation from R. Carrera et al. (2013). Uncertainties on the EW (20 per cent of relative uncertainty), on the *Gaia* photometry ($\pm$0.05 mag), on the distance of the star ($\pm$10 kpc), and on the polynomial coefficients from R. Carrera et al. (2013) have been folded into a Monte Carlo randomisation to derive accurate uncertainties on the metallicity. The estimated metallicity is $[Fe/H] = -2.70 \pm 0.21$, which is within the metallicity range estimated using the synthetic spectra. The comparison with the synthetic spectra and the EW-based method suggest that the star is likely not an UMP, although it is a VMP star. Further higher SNR spectroscopic follow-up observations, even with low-resolution, are needed to further investigate the nature of the remaining 8 UMP candidates in Canes Venatici II, Draco, and Sextans that we find in DESI DR1.

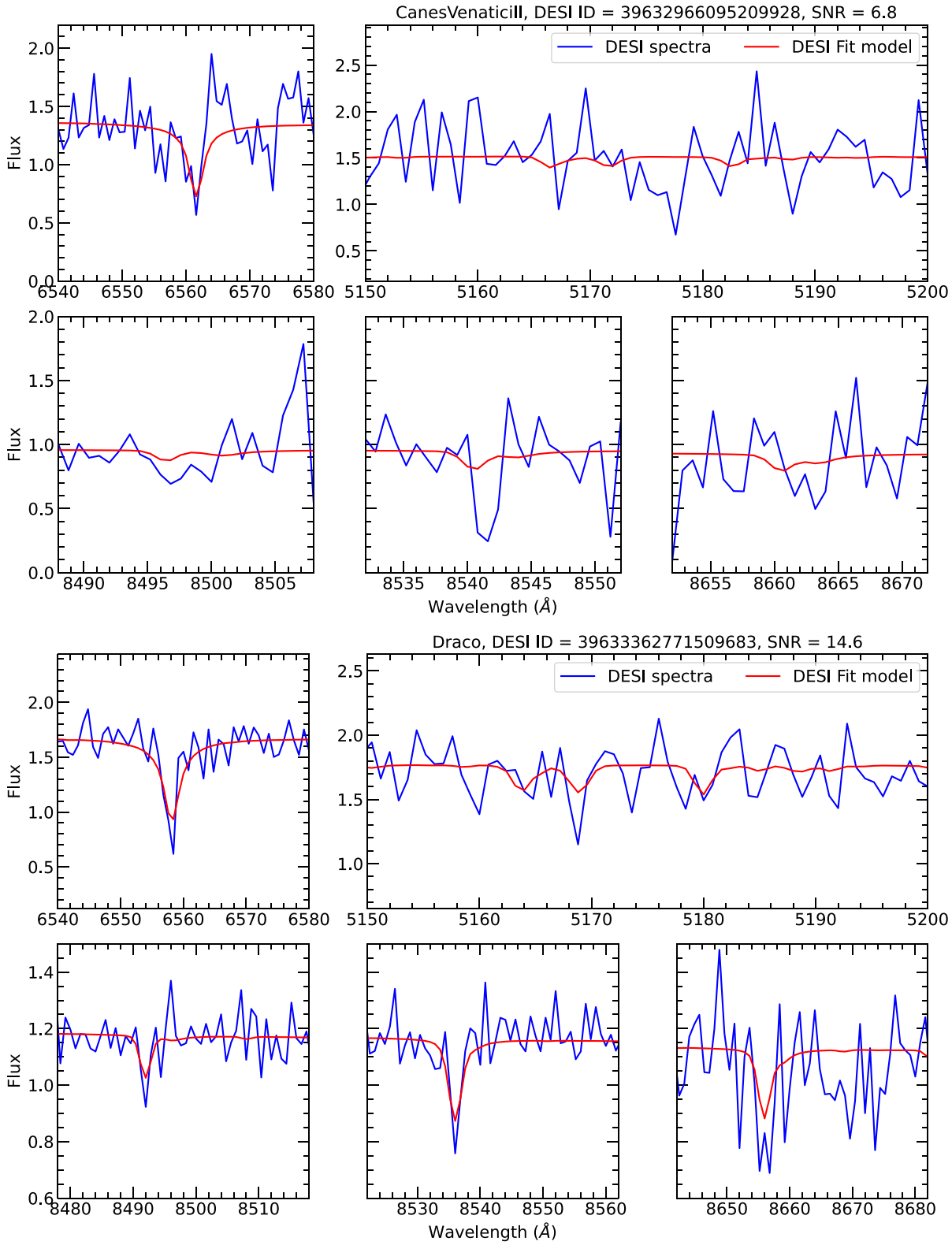

Figure 5. Spectra of candidate UMP stars, one in Canes Venatici II and one in Draco. DESI spectra and their spectral fitting models are shown in blue and red lines, respectively. Spectra are not corrected for radial velocity shifting nor flux normalized. For each star, the H α (top left), the Mg I Triplet (top right), and the Ca II Triplet (bottom row) spectral regions are displayed. Galaxy, DESI ID, and SNR are reported as title for each star.

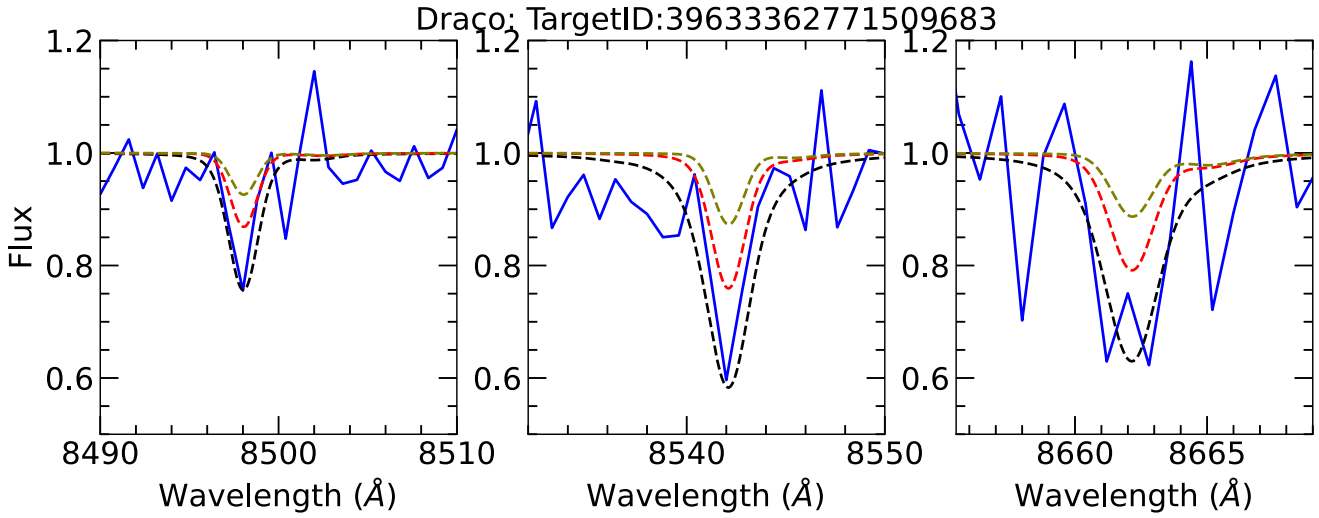

Figure 6. Calcium II Triplet lines for the UMP candidate in Draco with the highest SNR. Blue lines are the flux normalized DESI DR1 spectra. Olive, red, and black dashed lines are our synthetic spectra generated from MARCS models adopting [Ca/Fe] = +0.4; and [Fe/H] = −4.0, −3.0, and −2.0, respectively.

7 CONCLUSIONS

In this work, we explore the DESI DR1 catalogue to find stellar members in the Local Group dwarf galaxies. We cross-match DESI data with candidate members list from G. Battaglia et al. (2022) and A. B. Pace et al. (2022), which are based on the exquisite *Gaia* proper motion, on sky position and photometry. Together with radial velocities from DESI, we find stellar members in 15 galaxies, including ultra-faint dwarfs, classical dwarf galaxies, and irregular dwarfs (see Table 1). We also show that the candidate selection algorithms based on *Gaia* alone are doing a great job in removing foreground contaminations and in finding true stellar members (see Fig. 1 and Table 1), as the purity is $\gtrsim$ 96 per cent. In addition, we provide new members, that had low probability membership in either B22 and P22, but have DESI radial velocities in the range of five times the systemic velocity dispersion around the systemic RV values. These new members tend to be located in the outskirts of the systems. This indicates that *Gaia*-only based algorithms might miss the members in the extreme peripheries of dwarf galaxies, which can be recovered using spectroscopic information. In addition, two stars in the direction of DES J0225+0304 have similar values of radial velocities and proper motions. If they are true members of DES J0225+0304, then it leads to the first determination of the systemic radial velocity ($RV_{sys} = -150.0 \pm 7.0$ km s^{-1}).

The systems with the highest number of members in DESI are Draco and Sextans, and as it was not published before, we discuss chemodynamical properties within Sextans in detail (Section 5). Thanks to DESI, the member stars reach the outskirts of Sextans, up to $\sim 10\, r_h$ (Fig. 2). Our systemic velocity, systemic mean metallicity, and their dispersions are consistent with the literature's values (G. Battaglia et al. 2011; S. Koposov et al. 2026). The most metal-poor stars have a slightly higher velocity dispersion than the metal-rich group (Fig. 2), considering the [B22 + P22] sample. Within the galaxy, the velocity dispersion is lower in the inner regions, a behaviour that is opposite for the mean metallicity of the system (Fig. 3). These radial gradients suggest that the metal-rich population is kinematically colder and more confined in the inner parts of Sextans versus a kinematically hotter and more disperse metal-poor population. These results are also in line with the previous finding (e.g. G. Battaglia et al. 2011; E. Tolstoy et al. 2025), although they were not venturing in the extreme outskirts of Sextans. We find that the metallicity gradient is steeper in the inner regions (~ -0.25 dex r_h^{-1} or $\sim -12 \times 10^{-3}$ dex arcmin^{-1} or ~ -0.36 dex kpc^{-1}), while it flattens in the outskirts, reaching null values (see Fig. 3). The value of the metallicity gradient from DESI data and its behaviour are in agreement with previous findings using medium resolution spectroscopic analysis (G. Battaglia et al. 2011; E. Tolstoy et al. 2025). Moreover, the observational results are in good agreement with our chemodynamical simulation of a dwarf satellite galaxy that had no merger or tidal perturbation.

DESI DR1 also provides elemental abundances for some α−elements (see Fig. 4). The [(α, Mg, Ca)/Fe] for Sextans stars with [Fe/H] $\gtrsim -2.0$ are in line with the high-resolution spectroscopic literature data (W. Aoki et al. 2009; L. Mashonkina et al. 2017; R. Lucchesi et al. 2020; R. Theler et al. 2020; I. U. Roederer et al. 2023); however, Mg displays a large scatter in its elemental abundance. On the other hand, lower-metallicity stars show a large scatter of [(α, Mg, Ca)/Fe] (up to $\sim$ 2.5 dex for Mg) and an anticorrelation with [Fe/H], which is not seen in literature data, nor predicted by GCE models (C. Kobayashi et al. 2020a). Our revised GCE model for Sextans is in excellent agreement with the median [X/Fe] values of the literature data, reproducing the α−knee at [Fe/H] ~ -2.0, consistent with previous works (e.g. R. Theler et al. 2020). As warned by S. Koposov et al. (2026), the DESI's elemental abundance measurements (e.g. Mg and Ca) need updating; these elemental abundances are extremely useful for understanding the origin of each satellite galaxies.

Finally, we look for UMP candidate stars in the direction of the 15 Local Group galaxies observed by DESI DR1, selecting those stars with [Fe/H] $\lesssim -3.5$ and $\sigma_{[Fe/H]} \lesssim 1.0$ dex (Table 3). After careful inspection of their spectra (see Fig. 5 and 6), we find potentially 8 UMP candidates in Canes Venatici II (1 stars), Draco (2 stars) and Sextans (5 stars). Given their low SNR spectra, we are not able to firmly confirm or deny their UMP nature.

High SNR spectroscopic observations (SNR $\gtrsim$ 15), even with low-resolution, are needed for confirmation; new UMP members will be extremely valuable for understanding the chemical enrichment in the early Universe.

We are living at the beginning of an era in which various MOS instruments and surveys will observe thousands of stars in a glance for millions of objects in the Local Group. Subaru's PFS (N. Tamura et al. 2016; M. Chiba et al. 2026) and DESI already started acquiring data, while WEAVE (S. Jin et al. 2024) and 4MOST (R. S. de Jong et al. 2019) will soon start to operate. Similarly, in the next couple of decades, HRMOS (L. Magrini et al. 2023) and WST (V. Mainieri et al. 2024) will also play a crucial role in Galactic archaeology for measuring more accurate elemental abundances. To compare with theoretical predictions, it is necessary to put on the same scale the elemental abundances derived from the pipelines of the various MOS surveys, which can be done using those systems or stars observed by multiple surveys. For instance Sextans, studied here in details, or Draco, Ursa Minor are being observed by PFS and will be in the WEAVE footprint, as well as already present in DESI DR1. Elemental abundances in the most metal-poor stars are challenging to be derived, and dedicated pipelines within MOS surveys should be employed, as shown in this work.

ACKNOWLEDGEMENTS

The authors thank the anonymous referee for their insightful comments, which helped in improving the quality of the draft. FS and CK acknowledge funding from the UK Science and Technology Facilities Council through grant ST/Y001443/1. This work used the DiRAC Memory Intensive service (Cosma8 / Cosma7 / Cosma6 [∗]) at Durham University, managed by the Institute for Computational Cosmology on behalf of the STFC DiRAC HPC Facility (www.dirac.ac.uk). The DiRAC service at Durham was funded by BEIS, UKRI, and STFC capital funding, Durham University and STFC operations grants. DiRAC is part of the UKRI Digital Research Infrastructure.

This research used data obtained with the Dark Energy Spectroscopic Instrument (DESI). DESI construction and operations is managed by the Lawrence Berkeley National Laboratory. This material is based upon work supported by the U.S. Department of Energy, Office of Science, Office of High-Energy Physics, under Contract no. DE-AC02-05CH11231, and by the National Energy Research Scientific Computing Center, a DOE Office of Science User Facility under the same contract. Additional support for DESI was provided by the U.S. National Science Foundation (NSF), Division of Astronomical Sciences under Contract no. AST-0950945 to the NSF's National Optical-Infrared Astronomy Research Laboratory; the Science and Technology Facilities Council of the United Kingdom; the Gordon and Betty Moore Foundation; the Heising–Simons Foundation; the French Alternative Energies and Atomic Energy Commission (CEA); the National Council of Humanities, Science and Technology of Mexico (CONAHCYT); the Ministry of Science and Innovation of Spain (MICINN), and by the DESI Member Institutions: http://www.desi.lbl.gov/collaborating-institutions. The DESI collaboration is honored to be permitted to conduct scientific research on I'oligam Du'ag (Kitt Peak), a mountain with particular significance to the Tohono O'odham Nation. Any opinions, findings, and conclusions or recommendations expressed in this material are those of the author(s) and do not necessarily reflect the views of the U.S. National Science Foundation, the U.S. Department of Energy, or any of the listed funding agencies.

This work has made use of data from the European Space Agency (ESA) mission *Gaia* (https://www.cosmos.esa.int/gaia), processed by the *Gaia* Data Processing and Analysis Consortium (DPAC, https://www.cosmos.esa.int/web/gaia/dpac/consortium). Funding for the DPAC has been provided by national institutions, in particular the institutions participating in the *Gaia* Multilateral Agreement.

This research has made use of the SIMBAD database, operated at CDS, Strasbourg, France (M. Wenger et al. 2000). This work made extensive use of TOPCAT (M. B. Taylor 2005).

DATA AVAILABILITY

DESI DR1 data are publicly available, as well as candidate members from B22 and P22. The final list of members, which their number is reported in Table 1, will be publicly available as supplementary online material and at the CDS (cdsarc.cds.unistra.fr), once the paper is published. The original galactic chemical evolution model from C. Kobayashi et al. (2020a) is available at https://star.herts.ac.uk/~chiaki/gce, while the revised version is available upon reasonable request.

SUPPLEMENTARY MATERIAL

Supplementary data are available at *MNRAS* online.

Please note: Oxford University Press is not responsible for the content or functionality of any supporting materials supplied by the authors. Any queries (other than missing material) should be directed to the corresponding author for the article.

REFERENCES

Abdurro'uf et al., 2022, ApJS, 259, 35
Aguado D. S. et al., 2019, MNRAS, 490, 2241
Aihara H. et al., 2018, PASJ, 70, S4
Allende Prieto C., Beers T. C., Wilhelm R., Newberg H. J., Rockosi C. M., Yanny B., Lee Y. S., 2006, ApJ, 636, 804
Aoki W. et al., 2009, A&A, 502, 569
Ardern-Arentsen A. et al., 2024, MNRAS, 530, 3391
Arentsen A. et al., 2021, MNRAS, 505, 1239
Armandroff T. E., Da Costa G. S., 1991, AJ, 101, 1329
Arroyo-Polonio J. M., Pascale R., Battaglia G., Thomas G. F., Nipoti C., Vasiliev E., Tolstoy E., 2025, A&A, 699, A347
Battaglia G., Irwin M., Tolstoy E., Hill V., Helmi A., Letarte B., Jablonka P., 2008, MNRAS, 383, 183
Battaglia G., Tolstoy E., Helmi A., Irwin M., Parisi P., Hill V., Jablonka P., 2011, MNRAS, 411, 1013
Battaglia G., Taibi S., Thomas G. F., Fritz T. K., 2022, A&A, 657, A54
Beers T. C., Christlieb N., 2005, ARA&A, 43, 531
Benítez-Llambay A., Navarro J. F., Abadi M. G., Gottlöber S., Yepes G., Hoffman Y., Steinmetz M., 2016, MNRAS, 456, 1185
Bensby T. et al., 2019, The Messenger, 175, 35
Bettinelli M., Hidalgo S. L., Cassisi S., Aparicio A., Piotto G., 2018, MNRAS, 476, 71
Bonifacio P., Caffau E., François P., Spite M., 2025, A&A Rev., 33, 2
Bressan A., Marigo P., Girardi L., Salasnich B., Dal Cero C., Rubele S., Nanni A., 2012, MNRAS, 427, 127
Bullock J. S., Boylan-Kolchin M., 2017, ARA&A, 55, 343
Carlin J. L., Sand D. J., 2018, ApJ, 865, 7
Carrera R., Pancino E., Gallart C., del Pino A., 2013, MNRAS, 434, 1681
Chambers K. C. et al., 2016, The Pan-STARRS1 Surveys. preprint (arXiv:1612.05560)

Chiba M. et al., 2026, preprint (arXiv:2604.09875)
Chiti A. et al., 2021, Nat. Astron., 5, 392
Chiti A. et al., 2024, Nat. Astron., 8, 637
Chiti A. et al., 2026, Nat. Astron., 10, 830
Cicuéndez L., Battaglia G., 2018, MNRAS, 480, 251
Cooper A. P. et al., 2023, ApJ, 947, 37
DESI Collaboration, 2016, preprint (arXiv:1611.00036)
DESI Collaboration, 2024, AJ, 168, 58
Dalton G. et al., 2012, Proc. SPIE Conf. Ser. Vol. 8446, WEAVE: the next generation wide-field spectroscopy facility for the William Herschel Telescope. SPIE, Bellingham, p. 84460P
de Jong R. S. et al., 2019, The Messenger, 175, 3
Deason A. J., Bose S., Fattahi A., Amorisco N. C., Hellwing W., Frenk C. S., 2022, MNRAS, 511, 4044
Ding J. et al., 2025, ApJ, 994, 134
Drlica-Wagner A. et al., 2021, ApJS, 256, 2
El-Badry K. et al., 2018, MNRAS, 477, 1536
Fattahi A., Navarro J. F., Frenk C. S., Oman K. A., Sawala T., Schaller M., 2018, MNRAS, 476, 3816
Filion C., Wyse R. F. G., 2021, ApJ, 923, 218
Flores R. A., Primack J. R., 1994, ApJ, 427, L1
Frebel A., Bromm V., 2012, ApJ, 759, 115
Gaia Collaboration, 2016, A&A, 595, A1
Gaia Collaboration, 2018, A&A, 616, A1
Gaia Collaboration, 2023, A&A, 674, A1
Genina A. et al., 2018, MNRAS, 474, 1398
Grebel E. K., Gallagher J. S. III, Harbeck D., 2003, AJ, 125, 1926
Gustafsson B., Edvardsson B., Eriksson K., Jørgensen U. G., Nordlund Å., Plez B., 2008, A&A, 486, 951
Gwyn S. et al., 2025, AJ, 170, 324
Hartwig T., Ishigaki M. N., Kobayashi C., Tominaga N., Nomoto K., 2023, ApJ, 946, 20
Hastings W. K., 1970, Biometrika, 57, 97
Hayes C. R. et al., 2023, ApJ, 955, 17
Haywood M., Di Matteo P., Lehnert M. D., Katz D., Gómez A., 2013, A&A, 560, A109
Heger A., Woosley S. E., 2002, ApJ, 567, 532
Hendricks B., Koch A., Walker M., Johnson C. I., Peñarrubia J., Gilmore G., 2014, A&A, 572, A82
Hidalgo S. L. et al., 2013, ApJ, 778, 103
Higgs C. R., McConnachie A. W., Annau N., Irwin M., Battaglia G., Côté P., Lewis G. F., Venn K., 2021, MNRAS, 503, 176
Jensen J., Hayes C. R., Sestito F., McConnachie A. W., Waller F., Smith S. E. T., Navarro J., Venn K. A., 2024, MNRAS, 527, 4209
Ji A. P., Simon J. D., Frebel A., Venn K. A., Hansen T. T., 2019, ApJ, 870, 83
Jin S. et al., 2024, MNRAS, 530, 2688
Kazantzidis S., Łokas E. L., Callegari S., Mayer L., Moustakas L. A., 2011, ApJ, 726, 98
Kim B. et al., 2025, MNRAS, 540, 264
Kirby E. N. et al., 2010, ApJS, 191, 352
Kirby E. N., Lanfranchi G. A., Simon J. D., Cohen J. G., Guhathakurta P., 2011, ApJ, 727, 78
Kirby E. N., Cohen J. G., Guhathakurta P., Cheng L., Bullock J. S., Gallazzi A., 2013, ApJ, 779, 102
Klypin A., Kravtsov A. V., Valenzuela O., Prada F., 1999, ApJ, 522, 82
Kobayashi C., Nomoto K., 2009, ApJ, 707, 1466
Kobayashi C., Tsujimoto T., Nomoto K., 2000, ApJ, 539, 26
Kobayashi C., Springel V., White S. D. M., 2007, MNRAS, 376, 1465
Kobayashi C., Nomoto K., Hachisu I., 2015, ApJ, 804, L24
Kobayashi C., Leung S.-C., Nomoto K., 2020a, ApJ, 895, 138
Kobayashi C., Karakas A. I., Lugaro M., 2020b, ApJ, 900, 179
Koposov S. E. et al., 2024, MNRAS, 533, 1012
Koposov S. et al., 2026, Open J. Astrophys., 9, 55260
Lardo C. et al., 2021, MNRAS, 508, 3068
Limberg G., Placco V. M., Ji A. P., Yao Y., Chiti A., Mardini M. K., Frebel A., Rossi S., 2025, ApJ, 989, L18
Longeard N. et al., 2020, MNRAS, 491, 356
Longeard N. et al., 2022, MNRAS, 516, 2348
Longeard N. et al., 2023, MNRAS, 525, 3086
Longeard N., Jablonka P., Battaglia G., Malhan K., Martin N. F., Navarro J. F., Sestito F., 2025, A&A, 698, A63
Lucchesi R. et al., 2020, A&A, 644, A75
Luque E. et al., 2017, MNRAS, 468, 97
Magrini L. et al., 2023, preprint (arXiv:2312.08270)
Mainieri V. et al., 2024, preprint (arXiv:2403.05398)
Mashonkina L., Jablonka P., Sitnova T., Pakhomov Y., North P., 2017, A&A, 608, A89
McConnachie A. W., 2012, AJ, 144, 4
McConnachie A. W., Venn K. A., 2020, Res. Notes Am. Astron. Soc., 4, 229
Moore B., Ghigna S., Governato F., Lake G., Quinn T., Stadel J., Tozzi P., 1999, ApJ, 524, L19
Muñoz R. R., Côté P., Santana F. A., Geha M., Simon J. D., Oyarzún G. A., Stetson P. B., Djorgovski S. G., 2018, ApJ, 860, 66
Navarro J. F., Eke V. R., Frenk C. S., 1996, MNRAS, 283, L72
Nomoto K., Kobayashi C., Tominaga N., 2013, ARA&A, 51, 457
Norris J. E. et al., 2013, ApJ, 762, 28
Norris J. E., Yong D., Venn K. A., Gilmore G., Casagrande L., Dotter A., 2017, ApJS, 230, 28
Pace A. B., Erkal D., Li T. S., 2022, ApJ, 940, 136
Peñarrubia J., Navarro J. F., McConnachie A. W., 2008, ApJ, 673, 226
Poppett C. et al., 2024, AJ, 168, 245
Qi Y., Zivick P., Pace A. B., Riley A. H., Strigari L. E., 2022, MNRAS, 512, 5601
Reichert M., Hansen C. J., Hanke M., Skúladóttir Á., Arcones A., Grebel E. K., 2020, A&A, 641, A127
Revaz Y., Jablonka P., 2018, A&A, 616, A96
Riello M. et al., 2021, A&A, 649, A3
Roederer I. U., Pace A. B., Placco V. M., Caldwell N., Koposov S. E., Mateo M., Olszewski E. W., Walker M. G., 2023, ApJ, 954, 55
Sales L. V., Wetzel A., Fattahi A., 2022, Nat. Astron., 6, 897
Santos-Santos I. M. E., Frenk C. S., Navarro J. F., 2026, preprint (arXiv:2604.09539)
Sato K. S. et al., 2025, ApJ, 993, L7
Scannapieco C. et al., 2012, MNRAS, 423, 1726
Sestito F. et al., 2019, MNRAS, 484, 2166
Sestito F. et al., 2023a, MNRAS, 518, 4557
Sestito F., Roediger J., Navarro J. F., Jensen J., Venn K. A., Smith S. E. T., Hayes C., McConnachie A. W., 2023b, MNRAS, 523, 123
Sestito F. et al., 2023c, MNRAS, 525, 2875
Sestito F. et al., 2024a, A&A, 689, A201
Sestito F. et al., 2024b, A&A, 690, A333
Simon J. D., 2019, ARA&A, 57, 375
Skúladóttir Á. et al., 2021, ApJ, 915, L30
Skúladóttir Á. et al., 2023, The Messenger, 190, 19
Smith S. E. T. et al., 2023, AJ, 166, 76
Springel V., 2005, MNRAS, 364, 1105
Stancliffe R. J., 2009, MNRAS, 394, 1051
Starkenburg E. et al., 2010, A&A, 513, A34
Starkenburg E. et al., 2018, MNRAS, 481, 3838
Suda T. et al., 2008, PASJ, 60, 1159
Taibi S., Battaglia G., Leaman R., Brooks A., Riggs C., Munshi F., Revaz Y., Jablonka P., 2022, A&A, 665, A92
Takahashi K., Yoshida T., Umeda H., 2018, ApJ, 857, 111
Tamura N. et al., 2016, in Evans C. J., Simard L., Takami H., eds, Proc. SPIE Conf. Ser. Vol. 9908, Ground-based and Airborne Instrumentation for Astronomy VI. SPIE, Bellingham, p. 99081M
Tau E. A., Vivas A. K., Martínez-Vázquez C. E., 2024, AJ, 167, 57
Taylor M. B., 2005, in Shopbell P., Britton M., Ebert R., eds, ASP Conf. Ser. Vol. 347, Astronomical Data Analysis Software and Systems XIV. Astron. Soc. Pac., San Francisco, p. 29
The Dark Energy Survey Collaboration, 2005, preprint (astro-ph/0510346)
Theler R. et al., 2020, A&A, 642, A176
Tolstoy E., Hill V., Tosi M., 2009, ARA&A, 47, 371
Tolstoy E. et al., 2023, A&A, 675, A49

Tolstoy E. et al., 2025, A&A, 698, A53
Torrealba G. et al., 2019, MNRAS, 488, 2743
Umeda H., Nagele C., 2024, ApJ, 961, 146
Umeda H., Nomoto K., 2002, ApJ, 565, 385
van der Marel R. P., Fardal M., Besla G., Beaton R. L., Sohn S. T., Anderson J., Brown T., Guhathakurta P., 2012, ApJ, 753, 8
Venn K. A., Irwin M., Shetrone M. D., Tout C. A., Hill V., Tolstoy E., 2004, AJ, 128, 1177
Venn K. A. et al., 2012, ApJ, 751, 102
Vincenzo F., Kobayashi C., 2020, MNRAS, 496, 80
Vitali S. et al., 2022, MNRAS, 517, 6121
Vitali S. et al., 2025, A&A, 699, A163
Walker M. G., Peñarrubia J., 2011, ApJ, 742, 20
Walker M. G., Caldwell N., Mateo M., Olszewski E. W., Pace A. B., Bailey J. I., Koposov S. E., Roederer I. U., 2023, ApJS, 268, 19
Waller F. et al., 2023, MNRAS, 519, 1349
Wenger M. et al., 2000, A&AS, 143, 9
Wheeler C. et al., 2019, MNRAS, 490, 4447
Willman B. et al., 2005, ApJ, 626, L85
Yang Y., Hammer F., Jiao Y., Pawlowski M. S., 2022, MNRAS, 512, 4171
Yang H. et al., 2025, ApJ, 993, 249
York D. G. et al., 2000, AJ, 120, 1579
Youakim K. et al., 2017, MNRAS, 472, 2963
Zhang H.-X., Hunter D. A., Elmegreen B. G., Gao Y., Schruba A., 2012, AJ, 143, 47

APPENDIX A: HIGH-α STARS IN SEXTANS

Fig. 4 shows the presence of DESI DR1 stars with unusual high abundances of $\alpha-$elements. Stars with extremely high-α measurements are very rare among the observed stars. Given the anticorrelation of the DESI elemental abundances with metallicity, we retain unlikely the true high-α nature of these stars.

In the Sextans' literature, there are two stars from R. Theler et al. (2020) and one from I. U. Roederer et al. (2023) that stand out from the Sextans chemical distribution. One star, S05–95 (R. Theler et al. 2020), is extremely Mg-rich, with [Mg/Fe] $\sim +1.57$, although normal in Ca for that metallicity ([Ca/Fe] $\sim +0.25$). The authors reported a low SNR ($\lesssim 10$) for the spectrum of this star, also warning that [Mg/Fe] is measured only from one Mg I line (5528.410 Å, R. Theler et al. 2020). Another Mg-rich star is present in Sextans, J1008+0001 (I. U. Roederer et al. 2023), with [Mg/Fe] $\sim +1.84$ and [Ca/Fe] $\sim +0.5$. Extremely Mg-enriched stars do exist in Local Group dwarf galaxies; however, they are rare, e.g. 2 out of 61 observed stars in Sextans and 2 out of 45 observed stars in Ursa Minor (F. Sestito et al. 2023c).

The findings of such Mg-enhanced might be more frequent in low-mass ultra-faint dwarf galaxies, as also shown in A. P. Ji et al. (2019, e.g. BootesI, Coma Berenices, ReticulumII, SegueI, Ursa MajorII). This offers an explanation: the Mg-enhancement might be caused by inhomogeneous mixing star formation (e.g. A. Frebel & V. Bromm 2012). Alternatively, in case carbon is also enhanced, there are two scenarios. One related to the enrichment from a companion due to mass transfer (e.g. R. J. Stancliffe 2009), which would also increase s-process elemental abundances, observed as so-called CEMP-s stars (T. C. Beers & N. Christlieb 2005); another scenario is associated with enrichment from the primordial core-collapse supernovae (J. E. Norris et al. 2013), observed as so-called CEMP-no stars if neutron-capture elements are not enhanced (T. C. Beers & N. Christlieb 2005). No firm conclusions can be reached for S05–95, as elemental abundances for carbon are lacking. J1008+0001 is strongly enriched in C, Na, Si, and K, while it is deficient in the neutron-capture elements Sr, Ba and Eu. I. U. Roederer et al. (2023) classify this star as the first and, currently, the only CEMP-no discovered in Sextans.

The third star, S08–113 (R. Theler et al. 2020), is Ca-rich with [Ca/Fe] $\sim +1.05$ (from 12 Ca I lines), while it is Mg-poor, with [Mg/Fe] ~ -0.24. Similarly, the spectrum of this star had a low SNR; therefore, these elemental abundances should be taken with 'the grain of salt'. This combination of abundances might imply a high [Ca/Mg] ratio. One might think that such a high [Ca/Mg] ratio might be explained by the enrichment from pair-instability supernovae (PISNe; e.g. K. Nomoto et al. 2013); however, to firmly assess the nature of this star's progenitor, elemental abundances of the key elements of PISNe (Al, Na, Si, Zn, Cu, etc.) must be derived (e.g. A. Heger & S. E. Woosley 2002; H. Umeda & K. Nomoto 2002; K. Nomoto et al. 2013; K. Takahashi, T. Yoshida & H. Umeda 2018; H. Umeda & C. Nagele 2024).

This paper has been typeset from a TEX/LATEX file prepared by the author.